Lipotoxicity induces hepatic protein inclusions through TBK1-mediated p62/SQSTM1 phosphorylation.

Chun-Seok Cho[1*], Hwan-Woo Park[1,2*], Allison Ho[1], Ian A. Semple[1], Boyoung Kim[1], Insook Jang[1], Haeli Park[1], Shannon Reilly[1,3,4], Alan R. Saltiel[1,3,4], & Jun Hee Lee[1]

[1]Department of Molecular and Integrative Physiology, University of Michigan, Ann Arbor, MI 48109, USA; [2]Department of Cell Biology, Myunggok Medical Research Institute, Konyang University College of Medicine, Daejeon 35365, Republic of Korea; [3]Life Sciences Institute, University of Michigan, Ann Arbor, MI 48109, USA; [4]Institute for Diabetes and Metabolic Health, Departments of Medicine and Pharmacology, University of California, San Diego, La Jolla, CA 92093, USA

*These authors contributed equally to this work.

Supported by the NIH (R01DK102850 to J.H.L., T32GM008322 and T32AG000114 to A.H., R01DK060591 to A.R.S., and P30AG024824, P30DK034933, P30DK089503 and P30CA046592) and Korean NRF grants (2015R1A5A1009701 and 2015R1C1A1A01054654 to H.W.P.).

ADDRESS CORRESPONDENCE: Jun Hee Lee, Ph.D., Department of Molecular and Integrative Physiology, University of Michigan, 109 Zina Pitcher Pl., Ann Arbor, MI 48109-2200. E-mail: leeju@umich.edu, Tel: 734-764-6789

Abstract

Obesity commonly leads to hepatic steatosis, which often provokes lipotoxic injuries to hepatocytes that cause non-alcoholic steatohepatitis (NASH). NASH in turn is associated with the accumulation of insoluble protein aggregates that are composed of ubiquitinated proteins and ubiquitin adaptor p62/sequestosome 1 (SQSTM1). The formation of p62 inclusions in hepatocytes is the critical marker that distinguishes simple fatty liver from NASH and predicts a poor prognostic outcome for subsequent liver carcinogenesis. However, the molecular mechanism by which lipotoxicity induces protein aggregation is currently unknown. Here we show that upon saturated fatty acid-induced lipotoxicity, Tank-binding protein kinase 1 (TBK1) is activated and phosphorylates p62. The TBK1-mediated p62 phosphorylation is important for lipotoxicity-induced aggregation of ubiquitinated proteins and the formation of large protein inclusions in hepatocytes. In addition, cyclic GMP-AMP synthase (cGAS) and stimulator of interferon genes (STING), upstream regulators of TBK1, are involved in the lipotoxic activation of TBK1 and subsequent p62 phosphorylation in hepatocytes. Furthermore, TBK1 inhibition prevented formation of the ubiquitin-p62 aggregates, not only in cultured hepatocytes, but also in mouse models of obesity and NASH. These results suggest that lipotoxic activation of TBK1 and subsequent p62 phosphorylation are critical steps in the NASH pathology of protein inclusion accumulation in hepatocytes. This mechanism can provide an explanation for how hypernutrition and obesity promote the development of severe liver pathologies, such as steatohepatitis and liver cancer, by facilitating the formation of p62 inclusions.

Introduction

The incidence of obesity and its corresponding complications are increasing at an alarming rate.[1] Non-alcoholic fatty liver disease (NAFLD) is among many abnormalities associated with obesity and, in many patients, progresses to NASH.[2] While the precise molecular events involved in the development of NASH remain uncertain, it has been proposed that obesity-induced elevation in plasma free fatty acid levels provokes lipotoxic injuries to cells in the liver.[2] Saturated fatty acids (SFA) are major perpetrators of lipotoxic injuries to cells, while unsaturated fatty acids (UFA) often confer protection against SFA-induced lipotoxicity. NASH is characterized by various consequences of lipotoxic injury to liver cells, such as hepatocyte ballooning, protein inclusion formation, ectopic cell death, inflammation and fibrosis.[3-5] Obesity and NASH are also established risk factors for hepatocellular carcinoma (HCC).[6]

The formation of insoluble protein inclusions in hepatocytes is characteristic of a damaged liver for both mice and humans.[3-5,7-9] These inclusions are also the critical marker that distinguishes simple NAFLD from NASH[7,9] and consist primarily of ubiquitinated proteins such as keratins (KRT8/18) and the ubiquitin adaptor p62/SQSTM1.[3,8] Hepatic protein inclusions are closely linked to lipotoxic injuries and metabolic pathologies because they are frequently associated with fat droplet accumulation.[7] The mouse model of NASH, associated with large protein inclusions, is established by inducing obesity with a high fat diet (HFD) and administering additional insults that provoke inflammation, such as choline deficiency,[10,11] transgenic gene modulation,[5,12] or hepatotoxin administration.[5] However, HFD-induced obesity *per se*

is also sufficient to induce protein aggregates of ubiquitinated proteins and p62 that are insoluble in non-ionic detergents.[13-15] Although these findings suggest a causal link between obesity and hepatic protein aggregates, we currently have a very limited understanding of how obesity-associated lipotoxicity promotes the formation of insoluble protein inclusions. Acquiring this understanding is important especially because p62 accumulation in hepatocytes was recently demonstrated to facilitate obesity-associated liver fibrosis and HCC development.[12,16]

To investigate the mechanism of how protein aggregates are formed in NASH, we established an *in vitro* model in which SFAs, such as palmitic acid (PA) and stearic acid (SA), prominently induce insoluble inclusion bodies consisting of ubiquitinated proteins and p62 in the cytoplasm of human hepatoma HepG2 cells.[15] Using this system, as well as *in vivo* mouse models, we showed that attenuation of autophagic flux is one of the major causes of protein aggregate formation. In hepatocytes, obesity and SFA-induced lipotoxicity induce a prolonged elevation in cytosolic calcium, which interferes with the fusion between autophagosomes and lysosomes.[15] Interestingly, several stress signaling pathways, such as ER stress, oxidative stress, JNK and p53 pathways were not significantly involved in this protein inclusion process.[15]

Although autophagy inhibition may explain how protein inclusions can be formed upon lipotoxic injury, we observed that protein aggregates induced by simple autophagy inhibition were morphologically distinct from SFA- or obesity-induced protein inclusions. This histo-morphological discrepancy suggests that additional unknown pathways may mediate the formation of hepatic protein inclusions. Here, using both cultured cells and

animal models of lipotoxicity and obesity, we show that a signaling pathway leading to TBK1 activation induces phosphorylation and aggregation of p62, which facilitates the lipotoxicity-induced formation of ubiquitinated protein inclusions. Because inhibition of the TBK1 pathway effectively and specifically attenuates ubiquitin-p62 protein inclusions and fibrotic liver pathologies, this pathway could be a promising target for the treatment of NASH or other diseases associated with autophagy defects and proteinopathy.

Results

SFA induces large p62/SQSTM1 inclusions while other autophagy inhibitors do not. We and others have formerly shown that thapsigargin (Tg), bafilomycin A1 (Baf) and SFA interfere with autophagic flux, mainly through elevation of cytosolic calcium and subsequent inhibition of autophagosomal-lysosomal fusion.[15,17,18] However, we noticed that the patterns of p62 inclusions formed from SFA-induced lipotoxicity are apparently distinct from what we observed in Tg- and Baf-treated human hepatoma HepG2 cells. PA-induced protein aggregates appear as rod-shaped sizable inclusions in the cytoplasm (Fig. 1A), similar to hepatic protein inclusions observed during NASH[4] and NASH-associated HCC,[12] while Tg- or Baf-induced p62 aggregates are observed as numerous small puncta (Fig. 1A). This obvious difference suggests that, in addition to modulating the calcium signaling, lipotoxic insults modulate unknown target(s) that control the morphology of the p62-ubiquitin inclusion bodies.

The protein inclusions found in NASH are called Mallory-Denk bodies, which consist mainly of ubiquitinated KRT8/18 and p62.[3,8] Although we knew that the SFA-induced protein aggregates in HepG2 cells are enriched with p62 and ubiquitinated proteins (Fig. 1A-D),[19] we wanted to identify which specific proteins are found in this protein inclusion. Therefore, we isolated insoluble protein fractions from control and PA-treated cells, and subjected them to SDS-PAGE and Coomassie staining (Supporting Fig. S1A). Then, we searched for protein bands that were specifically enriched in PA-treated cells. From this analysis, we identified a ~54 kDa band as one of the most prominently enriched bands in the insoluble fraction from the PA-treated cells (Supporting Fig. S1A).

MS/MS analysis revealed that this band corresponds to KRT8 (Supporting Fig. S1A), supporting the close relationship between our PA-induced protein inclusions and the Mallory-Denk bodies. Therefore, this SFA-induced lipotoxicity model provides a pathophysiologically relevant experimental system for modeling NASH-associated protein inclusions.

SFA induces phosphorylation of p62 at Serine 403. p62 proteins accumulated under SFA-induced lipotoxicity exhibited strong electrophoretic mobility retardation (band shift; Fig. 1B), suggesting post-translational modification of the protein. Although the calcium channel blocker verapamil strongly suppressed p62 accumulation by restoring autophagic flux,[15] it did not inhibit the p62 band shift (Fig. 1B), suggesting that this modification is not controlled by calcium-autophagy signaling. To identify the nature of this modification, we immunoprecipitated p62 from SFA-treated cells and analyzed the protein with antibodies that detect various post-translational modifications.

Ubiquitination and acetylation signals were not detected in the region corresponding to p62 bands (Fig. 1C), but we did find a strong phosphorylation signal on Ser403 of p62 after SFA treatment (Fig. 1C). This corresponded to the shifted p62 bands (Fig. 1C). The gel shift was reduced by treatment with both lambda protein phosphatase and calf intestinal phosphatase (λPP+CIP; Supporting Fig. S1B). Phosphorylated p62 was almost exclusively found in insoluble fractions (Fig. 1D) and co-localized with the protein inclusions consisting of p62 (Fig. 1E) and ubiquitinated proteins (Fig. 1F). SFA-induced p62 shift and phosphorylation was also prominently observed in freshly isolated primary mouse hepatocytes (Supporting Fig. S1C).

Autophagy inhibition and subsequent p62 accumulation can promote casein kinase 2 (CK2)-dependent p62 phosphorylation at Ser403.[20] Autophagy inhibitors Tg and Baf, however, produced very weak p62 Ser403 phosphorylation, in contrast to the strong p62 phosphorylation induced upon SFA treatment (Supporting Fig. S1D,E). Tetrabromobenzotriazole (TBBt), a specific inhibitor of CK2,[20] did not inhibit SFA-induced p62 phosphorylation (Supporting Fig. S1F). These results indicate that neither autophagy inhibition nor CK2 is primarily responsible for the SFA-induced p62 phosphorylation. Consistent with this, SFA-induced p62 phosphorylation occurred earlier than its total protein accumulation (Supporting Fig. S1G), suggesting that this phosphorylation is not simply due to increased protein accumulation and is likely an active process.

TBK1 is activated upon SFA treatment. We then tested whether TBK1, another p62 Ser403 kinase,[21] is responsible for SFA-induced p62 phosphorylation. SFA strongly activated TBK1 in HepG2 cells (Fig. 2A), as monitored by activation loop phosphorylation (Ser172) of TBK1. In contrast to SFA, Tg and Baf only induced moderate activation of TBK1 (Fig. 2A), consistent with the p62 phosphorylation results (Supporting Fig. S1D,E). Calcium channel blockers verapamil and nicardipine did not inhibit SFA-induced TBK1 phosphorylation (Fig. 2B), although they strongly reduced p62 accumulation (Fig. 1B and 2B) by restoring autophagic flux.[15] Interestingly, UFA, such as oleic acid (OA) and docosahexaenoic acid (DHA), almost completely inhibited the action of SFA in activating TBK1 (Fig. 2C) and inducing p62 phosphorylation and accumulation (Fig. 2D).

In cells, activated TBK1 (p-TBK1) co-localized with phosphorylated p62 (p-p62; Fig. 2E) and total p62 (Fig. 2F) inclusions, suggesting that TBK1 may be the kinase responsible for the Ser403 phosphorylation of p62. However, unlike p-p62 that was predominantly found in the insoluble fraction (Fig. 1D), p-TBK1 was found in both soluble and insoluble fractions (Supporting Fig. S1H). One possibility is that TBK1 is present at the soluble side of the protein inclusion in order to efficiently phosphorylate p62 and assemble them into the insoluble inclusions. Consistent with this idea, PA-activated TBK1 phosphorylated p62 in an in vitro kinase assay (Supporting Fig. S1I) and can bind to endogenous p62 in reciprocal co-immunoprecipitation assays (Supporting Fig. S1J).

TBK1 is required for SFA-induced p62 phosphorylation and accumulation. We were curious if TBK1 actively promoted p62 phosphorylation and formation of ubiquitin-p62 aggregates in this lipotoxic context. Therefore, we used two recently discovered pharmacological inhibitors for TBK1, BX795[22] and amlexanox.[23] Both BX795 and amlexanox effectively suppressed SFA-induced p62 phosphorylation (Fig. 3A), supporting the hypothesis that TBK1 mediates the effect of SFA on p62 phosphorylation. Interestingly, SFA-induced accumulation of p62 and ubiquitinated proteins in insoluble fractions (Fig. 3A) and cytoplasmic inclusions (Fig. 3B) were also strongly inhibited, suggesting a relationship between p62 phosphorylation and protein inclusion formation.

Although BX795 and amlexanox are relatively specific inhibitors for TBK1, they may also inhibit other kinases such as PDK1 and IKKε.[22,23] To independently examine the role of TBK1, we used TBK1-specific shRNA constructs. shRNA-mediated silencing

of TBK1 almost completely inhibited the SFA-stimulated phosphorylation of p62 (Fig. 3C), indicating that TBK1 is indeed the major kinase that phosphorylates p62 in response to SFA. TBK1 silencing also prevented accumulation of insoluble p62 and ubiquitinated proteins (Fig. 3C), suggesting that the TBK1 activation and subsequent phosphorylation of p62 is responsible for accumulation of insoluble protein aggregates in SFA-treated cells.

The cGAS-STING axis is required for SFA-induced TBK1 activation. Next, we explored the mechanism of how TBK1 is activated upon lipotoxic insult during obesity. We focused on STING, a physiological activator of TBK1.[24] Unstimulated STING resides in the ER membrane, while upon stimulation with foreign DNA or cyclic dinucleotides, it translocates into an unknown cytoplasmic compartment where it interacts with TBK1 and induces TBK1 activation.[24] Notably, lipid composition of the ER membrane is dramatically altered during SFA-induced lipotoxicity,[25] and lipid modification (palmitoylation) of STING is required for its activation.[26] Under SFA-induced lipotoxicity, STING was found to co-localize with p-TBK1 (Fig. 4A), and shRNA-mediated silencing of STING substantially decreased SFA-induced TBK1 activation (Fig. 4A,B and Supporting Fig. S2A,B). STING silencing was also sufficient to prevent SFA-induced p62 phosphorylation and ubiquitin-p62 inclusions (Fig. 4B and Supporting Fig. S2A-D), supporting the idea that the STING-TBK1 axis mediates SFA-induced p62 phosphorylation and aggregation in hepatocytes.

Cyclic GMP-AMP (cGAMP), an upstream regulator of STING, can be synthesized in animal cells by the action of cGAMP synthase (cGAS). cGAS is activated

by the presence of cytoplasmic DNA, which could result from viral infection[27] or mitochondrial collapse.[28,29] Importantly, lipotoxic damage and NASH are associated with mitochondrial dysfunction and cytoplasmic leakage of mitochondrial DNA,[30,31] which can activate cGAS and subsequently the STING-TBK1 axis. Indeed, shRNA-mediated silencing of cGAS decreased SFA-induced TBK1 activation (Fig. 4C,D). cGAS silencing also inhibited p62 phosphorylation (Fig. 4D and Supporting Fig. S3A,B), STING translocation to the p-TBK1-positive compartment (Supporting Fig. S3C,D) and accumulation of ubiquitin-p62 inclusions (Fig. 4C,D and Supporting Fig. S3A-D). These results indicate that cGAS is necessary for SFA-induced activation of the STING-TBK1 axis and subsequent p62 phosphorylation and aggregation.

Although cGAS activation is necessary for activating the TBK1 axis during SFA-induced lipotoxicity, it was not sufficient for inducing p62 inclusion. For instance, TBK1 activation by extracellular cGAMP[27] (Supporting Fig. S4A) did not provoke p62 phosphorylation and accumulation in cells (Supporting Fig. S4B). Therefore, activation of additional SFA-induced signaling pathways seems to be necessary for TBK1 to properly induce p62 phosphorylation and aggregation.

We tested whether the requirement of STING and cGAS for activating the TBK1-p62 axis could be replicated in primary mouse hepatocytes, using *Sting*- and *cGas*-knockout mice.[27] As observed in HepG2 cells, PA-induced lipotoxicity in wild-type (WT) mouse hepatocytes triggered strong phosphorylation of TBK1 (Supporting Fig. S5A) and p62 (Supporting Fig. S5B) in protein inclusions. However, primary hepatocytes isolated from *Sting*- and *cGas*-knockout mice exhibited dramatic attenuation of these

processes in both immunostaining (Supporting Fig. S5A,B) and immunoblotting (Supporting Fig. S5C-F) experiments. These results support the requirement of the cGAS-STING axis in lipotoxicity-induced TBK1 activation and subsequent induction of p62-ubiquitinated protein inclusions.

TBK1 controls Nrf2 targets and autophagic flux. Excessive accumulation of p62 can upregulate the Nrf2 transcription factor because p62 inhibits Keap1, an Nrf2 suppressor.[32] *SQSTM1*, the gene encoding p62, is also a transcriptional target of Nrf2; therefore, p62 accumulation leads to further upregulation of p62 expression, forming a positive feedback loop.[32] Consistent with this pathway, SFA induced strong expression of Nrf2 target genes including *SRX*, *NQO1*, *GSTA1* and *SQSTM1* (Supporting Fig. S6A-D). Silencing of *cGAS*, *STING* or *TBK1* abolished the lipotoxicity-induced Nrf2 target gene expression (Supporting Fig. S6A-D), while silencing of p62/SQSTM1 did not inhibit the lipotoxicity-induced TBK1 activation (Supporting Fig. S6E). These results indicate that, in the context of lipotoxicity, TBK1 acts as an upstream regulator of p62 and other Nrf2 target genes.

As we formerly reported,[15] PA-induced lipotoxicity provoked an almost complete segregation between an autophagosome marker LC3 and a lysosomal marker LAMP1 (Supporting Fig. S7A,B), indicating a strong autophagy arrest at the autophagosomal-lysosomal fusion step. TBK1 inhibitors, BX795 and amlexanox, were able to substantially restore the co-localization between the LC3 and LAMP1 (Supporting Fig. S7A,B), indicating that they can at least partially resume autophagic flux during lipotoxicity. As a result of efficient lysosomal fusion and subsequent degradation, the

level of LC3-positive autophagosomes was reduced by the TBK1 inhibitors (Supporting Fig. S7C). It is possible that reduced p62 expression and aggregation during TBK1 inhibition may have lessened the autophagy overload and thereby alleviated the autophagic defects. The restoration of autophagic flux may have further contributed to efficient elimination of p62 and ubiquitinated protein inclusions (Fig. 3) as a positive feedback.

TBK1 inhibition suppresses protein inclusions in livers of obese mice. Next, we examined if TBK1 is important for p62 control *in vivo* during HFD-induced fatty liver.[13-15] As observed in SFA-treated HepG2 cells, insoluble p62 induced by HFD was phosphorylated at Ser403 (Fig. 5A). Ten days of TBK1 inhibition by BX795 administration was sufficient to reduce this phosphorylation, suggesting a mechanistic role of TBK1 in HFD-induced p62 phosphorylation (Fig. 5A). The level of p62 and ubiquitinated proteins in hepatic inclusion bodies was also dramatically reduced to the level of pre-obese conditions (Fig. 5A,B), indicating that TBK1 is indeed important for p62 regulation during obesity. However, BX795 was also found to substantially reduce body weight without altering food intake (Supporting Fig. S8A,B). Because systemic TBK1 inhibition is known to control energy metabolism and inflammation through adipose tissues,[23,33] it is possible that these inhibitors corrected the HFD-induced protein inclusion pathologies indirectly through suppression of obesity and normalization of metabolism.

To address this issue, we generated liver-specific TBK1-knockout (L-*Tbk1*-KO) mice by crossing *Tbk1*$^{F/F}$ mice with the *Albumin-Cre* strain. As expected, L-*Tbk1*-KO

mice exhibited dramatically reduced expression of both p-TBK1 and TBK1 in the liver tissue (Fig. 5C). However, HFD-induced body weight gain was almost the same between L-*Tbk1*-KO mice and L-*Tbk1*-WT (*Tbk1*$^{F/F}$; littermate control) mice (Supporting Fig. S8C,D), suggesting that the effect of liver-specific TBK1 loss on general metabolism is minimal. Then, we analyzed the effect of L-*Tbk1*-KO on hepatic protein inclusions. Despite the minimal effects on obesity development (Supporting Fig. S8C,D), liver-specific TBK1 deletion dramatically reduced p62 phosphorylation (Fig. 5C), as well as accumulation of p62 and ubiquitinated proteins in insoluble inclusion bodies (Fig. 5C,D). These results demonstrate that TBK1 is indeed critical for obesity-induced p62 phosphorylation and subsequent formation of ubiquitin-p62 inclusions.

TBK1 inhibition reduces p62 inclusions and liver fibrosis during NASH. Although HFD induces modest p62 inclusion formation (Fig. 5A,B),[13-15] HFD feeding in WT mice did not produce typical NASH pathologies such as active steatohepatitis or fibrotic lesions.[34] Therefore, HFD is combined with additional insults, such as nutritional deficiency[10,11] or expression of foreign proteins[5,12] to induce a stronger NASH phenotype. These NASH models often produce much stronger accumulation of p62 and ubiquitinated proteins when compared to the simple HFD model.[5] Therefore, we tested the role of TBK1 in a more severe NASH model, induced by a methionine-restricted choline-deficient (CD)-HFD,[11] which recapitulates many of the human NASH pathologies.[11] These include severe hepatosteatosis and liver fibrosis (Supporting Fig. S9A), attenuated weight gain (Supporting Fig. S9B), and extensive liver damage

(Supporting Fig. S9C). These pathologies were strongly suppressed by dietary supplementation of choline and methionine (CS-HFD; Supporting Fig. S9A-C).

We found that this CD-HFD model produced much stronger accumulation of phosphorylated p62 proteins (Fig. 6A), compared to the LFD or CS-HFD control animals (Supporting Fig. S9D). Correspondingly, the accumulation of p62 and ubiquitinated proteins was also very pronounced in the CD-HFD model (Fig. 6A and Supporting Fig. S9D).

As observed in the simple HFD model (Fig. 5A), a 10-day treatment of the TBK1 inhibitor BX795 was sufficient to suppress the p62 phosphorylation and accumulation, as well as ubiquitinated protein inclusions (Fig. 6A) in the CD-HFD model. In this case, reduction in p62 inclusions was not associated with any significant changes in body weight (Supporting Fig. S9E) or the level of hepatic fat accumulation (Fig. 6B and Supporting Fig. S9F). The levels of liver damage (Fig. 6C), hepatocyte cell death (Fig. 6D and Supporting Fig. S9F) and hepatic macrophage infiltration (Fig. 6D,E) were also comparable between BX795-untreated and -treated groups.

However, interestingly, we found that the CD-HFD-induced expression of inflammatory cytokines, such as TNF1, IL6 and IL10, was substantially suppressed by BX795 treatment (Supporting Fig. S9G). Furthermore, the level of liver fibrosis, monitored through Sirius Red staining (Fig. 7A,B) and α-smooth muscle actin expression (Fig. 7A-E), was substantially reduced by the BX795 treatment. Other markers of liver fibrosis, such as collagen levels (COL1A1 and COL3A1) and pro-fibrogenic markers of

hepatic stellate cells (e.g. MMPs, TIMPs, LOX, CTGF and PECAM1) were also induced by CD-HFD and suppressed by BX795 treatment (Fig. 7C-E).

TBK1 inhibition reduces NASH-associated ROS accumulation. Suppression of TBK1 and subsequent inhibition of p62 protein inclusions (Fig. 6A,B) did not alleviate liver damage and hepatocyte death (Fig. 6C,D). However, since TBK1 inhibition strongly reduced fibrotic pathologies (Fig. 7A-E), it is still possible that hepatic p62 protein inclusions somehow contribute to fibrotic pathologies by inducing sublethal damages in hepatocytes. One such hepatocyte-originated signal is reactive oxygen species (ROS) that provoke hepatic stellate cell activation.[35,36] Indeed, in a recent report, hepatocyte-specific knockout of p62, which inhibits protein inclusion formation, strongly suppressed ROS accumulation and fibrosis during NASH.[12] We tested if TBK1 inhibition, which suppresses p62 inclusion (Fig. 6A,B), can also reduce ROS accumulation during CD-HFD-induced NASH. ROS visualization using dihydroethidium (DHE) revealed that, as expected, CD-HFD prominently upregulated liver ROS level, while BX795 treatment strong antagonized the effect of CD-HFD (Fig. 8A,B). Therefore, TBK1 inhibition effectively suppressed hepatic oxidative stress and fibrosis during NASH.

STING is involved in HFD-induced p62 phosphorylation. We then tested the genetic involvement of the cGAS-STING pathway in the mouse NASH models. Upon the simple HFD treatment, *Sting*-KO mice produced less p62 phosphorylation and accumulation when compared to WT mice (Supporting Fig. S10A,B) without significant effects on obesity development (Supporting Fig. S10D,E). Accumulation of ubiquitinated proteins was also much less pronounced in *Sting*-KO mice (Supporting Fig. S10A,C), suggesting

a role for STING in the p62 phosphorylation and protein inclusion processes. However, under the CD-HFD treatment, the effect of STING loss was not detectable (Supporting Fig. S10F-H). Therefore, even though the cGAS-STING pathway plays important roles in activating TBK1 upon lipotoxic stimuli, other types of metabolic insults such as choline deficiency and liver damage can activate additional independent signaling pathway(s) that can provoke activation of the TBK1-p62 signaling.

Discussion

The hepatocyte protein inclusion is one of the most prominent histopathological features of diseased hepatocytes in fatty liver,[3-5,7-9] in addition to steatosis and cell death. The association between fatty liver pathologies and inclusion bodies has been known for around 100 years, and ubiquitinated proteins and p62/SQSTM1 were more recently shown to be the major components.[3,8] Still, whether these p62 inclusions indeed play a pathogenetic role, and the mechanisms of how these inclusion bodies form during lipotoxic injuries largely remained elusive until very recently. In addition to recent studies that showed the pathogenetic role for p62 inclusions during autophagy inhibition, NASH and HCC,[12,37] our current study provides a mechanism for how p62 protein inclusions can form inside lipid-laden hepatocytes during fatty liver and NASH.

We demonstrate here for the first time that SFA- or obesity-induced lipotoxicity promotes protein inclusion formation through activation of the TBK1 signaling pathway. Also referred to as the xenophagy pathway, the TBK1 axis has been known to facilitate autophagic elimination of invading microorganisms in macrophages (Fig. 8C).[21] In this process, TBK1, activated by bacterially-derived LPS, cyclic dinucleotides or DNA, phosphorylates p62 at Ser403 and subsequently promotes its association with ubiquitinated bacterial proteins, forming bacteria-p62 aggregates that are destined for autophagic degradation. Here we revealed that the same pathway plays a distinct pathogenetic role in hepatocytes during obesity-associated NASH. Upon lipotoxic insults, TBK1 is activated by the cGAS-STING pathway, as well as by unknown signaling mediators (Fig. 8D). The activated TBK1 phosphorylates p62 at Ser403, promoting the

formation of ubiquitinated protein inclusions. Although this process normally functions to prepare ubiquitinated proteins for autophagic degradation, obesity and lipotoxic injuries interfere with autophagic flux through an independent mechanism.[13,15] Therefore, protein inclusions that cannot be degraded by either autophagy or proteasomal pathways accumulate and grow larger in size. p62 phosphorylation and accumulation further upregulates p62 expression through Nrf2-mediated positive feedback,[32] which aggravates autophagy overload and malfunctioning. These results provide a mechanistic explanation of how p62 inclusions form during lipotoxic injuries and fatty liver. Even though more studies need to be done on how these inclusions are mechanistically associated with other pathological features of NASH, we believe that this study, delineating the mechanisms of how lipotoxic injuries provoke p62 protein inclusions, is an important advance in the field of NASH and fatty liver diseases.

Because p62 is known to regulate redox homeostasis, nutrient signaling and carcinogenic processes,[16] lipotoxic p62 phosphorylation and accumulation may play additional pathogenetic roles in fatty liver disease. Indeed, our results indicate that TBK1 inhibition, which suppresses p62 phosphorylation and accumulation, can specifically restore liver ROS accumulation and subsequent fibrotic pathologies in a NASH model induced by CD-HFD. However, other NASH-associated pathologies, such as hepatosteatosis, hepatocyte damage and macrophage infiltration, were not altered by TBK1 inhibition in this model. Interestingly, recent studies of hepatocellular p62 indicated that hepatocyte-specific p62 knockout mice, which do not form hepatic protein inclusions, showed the exact same phenotype; p62 ablation suppressed liver ROS and

fibrosis without alleviating hepatosteatosis during NASH.[12] Because both TBK1 inhibition and p62 ablation suppresses protein inclusion formation, oxidative stress and fibrosis, it is plausible that the protein inclusions play a pathogenetic role in redox imbalance and subsequent fibrotic progression. For instance, aberrant accumulation of protein inclusions and subsequent block of autophagy can impair the clearance of dysfunctional mitochondria that produce pathogenic levels of ROS. However, the exact mechanism for how p62 inclusions provoke a redox imbalance in the liver during NASH was not provided by either the former studies or the current study. Therefore, future investigation should work towards extensively understanding this potential mechanism. In addition, considering that TBK1 has a well-established role in regulating inflammatory signaling,[38] it is possible that the observed effects on liver fibrosis were mediated through p62-independent mechanisms in non-hepatocytes such as macrophages or hepatic stellate cells. Although damaged hepatocytes are among the major sources of ROS during NASH, other cell types such as immune cells could also contribute to the ROS production.[36] Therefore, even though it is likely that hepatic protein inclusions are specific promoters of liver fibrosis and that TBK1 is a central signaling component for this NASH-promoting process, alternative explanations are possible through the role of TBK1-expressing non-hepatocytes (Fig. 8D).

Excessive p62 protein inclusions in NASH predisposes a patient to HCC progression, and HCC with prominent p62 inclusions predicts a poor prognostic outcome.[12,39,40] Therefore, the p62 protein inclusions may also have a role in promoting liver cancer. Indeed, recent animal studies established that the homeostatic maintenance

of p62 levels in liver tumors and tumor microenvironments is important for suppressing hepatocarcinogenesis.[12,16,32,41] Specifically, p62 accumulation in hepatocytes promotes HCC development during NASH,[12] while endogenous p62 in hepatic stellate cells suppresses HCC by modulating the tumor microenvironment.[41] Since our results show that obesity-activated TBK1 signaling plays a critical role in producing p62 inclusion accumulation in hepatocytes during lipotoxicity, it may provide the molecular conduit of how hypernutrition and obesity can promote NASH-associated development of HCC.[6]

It should be noted that pharmacological TBK1 inhibition was recently shown to alleviate NAFLD and insulin resistance in both humans and mice,[23,42] which is likely to be mediated by the inflammation-regulating role of TBK1 in adipose tissues and macrophages.[23,33,38] In addition to these well-established roles in inflammation, our current study shows that TBK1 also plays an important role for protein homeostasis in hepatocytes through regulating p62 phosphorylation. TBK1 inhibition and subsequent suppression of hepatic protein inclusions might also contribute to restoring liver redox homeostasis and attenuating fibrotic disease progression. Therefore, further investigation about how the TBK1 pathway is regulated by lipotoxic insults and how TBK1 regulation in different tissues affects various pathologies in NASH may bring about a new paradigm for understanding NAFLD, as well as other similar types of liver diseases that present with the disruption of protein homeostasis.

Materials and Methods

Cell culture studies. HepG2 cells were obtained from ATCC (HB-8065). Primary hepatocytes were isolated and cultured as previously described.[34] To induce lipotoxicity, de-lipidated low-endotoxin BSA was loaded with PA and other fatty acids, as formerly described,[15,34] and applied to cultured cells. Details in cell culture procedures are described in Supporting Information.

Animal studies. Mice of C57BL/6 genetic background were used for this study. All animal studies were ethically approved and overseen by the University Committee on Use and Care of Animals (UCUCA) at the UM. Details in animal procedures, including mouse genotypes and their sources, number, age and gender of mice, diet treatment and drug administration, are described in Supporting Information and corresponding Figure Legends.

Quantification and statistics. Immunoblot images were quantified by densitometry, and protein expressions were expressed as relative band intensities. Co-localization of different proteins was expressed as line-scan evaluation graph or Pearson's coefficient. All the statistical analyses were performed with more than three independent biological replicates ($n \geq 3$) for cell culture studies or with the indicated numbers of animals for *in vivo* mouse studies. Statistical significance of differences between two groups was calculated using a Student's *t* test (*, $P<0.05$; **, $P<0.01$; ***, $P<0.001$).

Other methods. For details of reagents, lentiviral constructs, subcellular fractionation, protein analysis, immunocytochemistry and histology, see Supporting Information.

Acknowledgements

We thank Drs. L. Yin and D. Zhang for primary hepatocyte isolation. We thank Drs. M.B. Omary and S. Hwang (Univ. of Chicago), and Lee lab members for their insightful comments. We also thank Drs. R.A. Miller and S. Pletcher for access to lab equipment and Santa Cruz Biotech Inc. for sharing reagents.

References

1. Scherer PE, Hill JA. Obesity, Diabetes, and Cardiovascular Diseases: A Compendium. Circ Res 2016;118:1703-1705.

2. Cusi K. Role of obesity and lipotoxicity in the development of nonalcoholic steatohepatitis: pathophysiology and clinical implications. Gastroenterology 2012;142:711-725 e716.

3. Zatloukal K, Stumptner C, Fuchsbichler A, Heid H, Schnoelzer M, Kenner L, Kleinert R, et al. p62 Is a common component of cytoplasmic inclusions in protein aggregation diseases. Am J Pathol 2002;160:255-263.

4. Strnad P, Nuraldeen R, Guldiken N, Hartmann D, Mahajan V, Denk H, Haybaeck J. Broad spectrum of hepatocyte inclusions in humans, animals, and experimental models. Compr Physiol 2013;3:1393-1436.

5. Kucukoglu O, Guldiken N, Chen Y, Usachov V, El-Heliebi A, Haybaeck J, Denk H, et al. High-fat diet triggers Mallory-Denk body formation through misfolding and crosslinking of excess keratin 8. Hepatology 2014;60:169-178.

6. Marengo A, Rosso C, Bugianesi E. Liver Cancer: Connections with Obesity, Fatty Liver, and Cirrhosis. Annu Rev Med 2016;67:103-117.

7. Caldwell S, Ikura Y, Dias D, Isomoto K, Yabu A, Moskaluk C, Pramoonjago P, et al. Hepatocellular ballooning in NASH. J Hepatol 2010;53:719-723.

8. Stumptner C, Fuchsbichler A, Heid H, Zatloukal K, Denk H. Mallory body--a disease-associated type of sequestosome. Hepatology 2002;35:1053-1062.

9. Brunt EM, Tiniakos DG. Histopathology of nonalcoholic fatty liver disease. World J Gastroenterol 2010;16:5286-5296.

10. Rinella ME, Elias MS, Smolak RR, Fu T, Borensztajn J, Green RM. Mechanisms of hepatic steatosis in mice fed a lipogenic methionine choline-deficient diet. J Lipid Res 2008;49:1068-1076.

11. Matsumoto M, Hada N, Sakamaki Y, Uno A, Shiga T, Tanaka C, Ito T, et al. An improved mouse model that rapidly develops fibrosis in non-alcoholic steatohepatitis. Int J Exp Pathol 2013;94:93-103.

12. Umemura A, He F, Taniguchi K, Nakagawa H, Yamachika S, Font-Burgada J, Zhong Z, et al. p62, Upregulated during Preneoplasia, Induces Hepatocellular Carcinogenesis by Maintaining Survival of Stressed HCC-Initiating Cells. Cancer Cell 2016;29:935-948.

13. Gonzalez-Rodriguez A, Mayoral R, Agra N, Valdecantos MP, Pardo V, Miquilena-Colina ME, Vargas-Castrillon J, et al. Impaired autophagic flux is associated with increased endoplasmic reticulum stress during the development of NAFLD. Cell Death Dis 2014;5:e1179.

14. Yang L, Li P, Fu S, Calay ES, Hotamisligil GS. Defective hepatic autophagy in obesity promotes ER stress and causes insulin resistance. Cell Metab 2010;11:467-478.

15. Park HW, Park H, Semple IA, Jang I, Ro SH, Kim M, Cazares VA, et al. Pharmacological correction of obesity-induced autophagy arrest using calcium channel blockers. Nat. Commun. 2014;5:4834.

16. Moscat J, Karin M, Diaz-Meco MT. p62 in Cancer: Signaling Adaptor Beyond Autophagy. Cell 2016;167:606-609.

17. Ganley IG, Wong PM, Gammoh N, Jiang X. Distinct autophagosomal-lysosomal fusion mechanism revealed by thapsigargin-induced autophagy arrest. Mol Cell 2011;42:731-743.

18. Mauvezin C, Neufeld TP. Bafilomycin A1 disrupts autophagic flux by inhibiting both V-ATPase-dependent acidification and Ca-P60A/SERCA-dependent autophagosome-lysosome fusion. Autophagy 2015;11:1437-1438.

19. Park HW, Lee JH. Calcium channel blockers as potential therapeutics for obesity-associated autophagy defects and fatty liver pathologies. Autophagy 2014;10:2385-2386.

20. Matsumoto G, Wada K, Okuno M, Kurosawa M, Nukina N. Serine 403 phosphorylation of p62/SQSTM1 regulates selective autophagic clearance of ubiquitinated proteins. Mol Cell 2011;44:279-289.

21. Pilli M, Arko-Mensah J, Ponpuak M, Roberts E, Master S, Mandell MA, Dupont N, et al. TBK-1 promotes autophagy-mediated antimicrobial defense by controlling autophagosome maturation. Immunity 2012;37:223-234.

22. Clark K, Plater L, Peggie M, Cohen P. Use of the pharmacological inhibitor BX795 to study the regulation and physiological roles of TBK1 and IkappaB kinase epsilon: a distinct upstream kinase mediates Ser-172 phosphorylation and activation. J Biol Chem 2009;284:14136-14146.

23. Reilly SM, Chiang SH, Decker SJ, Chang L, Uhm M, Larsen MJ, Rubin JR, et al. An inhibitor of the protein kinases TBK1 and IKK-varepsilon improves obesity-related metabolic dysfunctions in mice. Nat Med 2013;19:313-321.

24. Barber GN. STING-dependent cytosolic DNA sensing pathways. Trends Immunol 2014;35:88-93.

25. Fu S, Watkins SM, Hotamisligil GS. The role of endoplasmic reticulum in hepatic lipid homeostasis and stress signaling. Cell Metab 2012;15:623-634.

26. Mukai K, Konno H, Akiba T, Uemura T, Waguri S, Kobayashi T, Barber GN, et al. Activation of STING requires palmitoylation at the Golgi. Nat Commun 2016;7:11932.

27. Cai X, Chiu YH, Chen ZJ. The cGAS-cGAMP-STING pathway of cytosolic DNA sensing and signaling. Mol Cell 2014;54:289-296.

28. West AP, Khoury-Hanold W, Staron M, Tal MC, Pineda CM, Lang SM, Bestwick M, et al. Mitochondrial DNA stress primes the antiviral innate immune response. Nature 2015;520:553-557.

29. Rongvaux A, Jackson R, Harman CC, Li T, West AP, de Zoete MR, Wu Y, et al. Apoptotic caspases prevent the induction of type I interferons by mitochondrial DNA. Cell 2014;159:1563-1577.

30. Garcia-Martinez I, Santoro N, Chen Y, Hoque R, Ouyang X, Caprio S, Shlomchik MJ, et al. Hepatocyte mitochondrial DNA drives nonalcoholic steatohepatitis by activation of TLR9. J Clin Invest 2016;126:859-864.

31. Rolo AP, Teodoro JS, Palmeira CM. Role of oxidative stress in the pathogenesis of nonalcoholic steatohepatitis. Free Radic Biol Med 2011.

32. Katsuragi Y, Ichimura Y, Komatsu M. Regulation of the Keap1-Nrf2 pathway by p62/SQSTM1. Current Opinion in Toxicology 2016;1:54-61.

33. Reilly SM, Ahmadian M, Zamarron BF, Chang L, Uhm M, Poirier B, Peng X, et al. A subcutaneous adipose tissue-liver signalling axis controls hepatic gluconeogenesis. Nat Commun 2015;6:6047.

34. Park HW, Park H, Ro SH, Jang I, Semple IA, Kim DN, Kim M, et al. Hepatoprotective role of Sestrin2 against chronic ER stress. Nat Commun 2014;5:4233.

35. Friedman SL. Mechanisms of hepatic fibrogenesis. Gastroenterology 2008;134:1655-1669.

36. Parola M, Robino G. Oxidative stress-related molecules and liver fibrosis. J Hepatol 2001;35:297-306.

37. Komatsu M, Waguri S, Koike M, Sou YS, Ueno T, Hara T, Mizushima N, et al. Homeostatic levels of p62 control cytoplasmic inclusion body formation in autophagy-deficient mice. Cell 2007;131:1149-1163.

38. Yu T, Yi YS, Yang Y, Oh J, Jeong D, Cho JY. The pivotal role of TBK1 in inflammatory responses mediated by macrophages. Mediators Inflamm 2012;2012:979105.

39. Aigelsreiter A, Neumann J, Pichler M, Halasz J, Zatloukal K, Berghold A, Douschan P, et al. Hepatocellular carcinomas with intracellular hyaline bodies have a poor prognosis. Liver Int 2017;37:600-610.

40. Bao L, Chandra PK, Moroz K, Zhang X, Thung SN, Wu T, Dash S. Impaired autophagy response in human hepatocellular carcinoma. Exp Mol Pathol 2014;96:149-154.

41. Duran A, Hernandez ED, Reina-Campos M, Castilla EA, Subramaniam S, Raghunandan S, Roberts LR, et al. p62/SQSTM1 by Binding to Vitamin D Receptor Inhibits Hepatic Stellate Cell Activity, Fibrosis, and Liver Cancer. Cancer Cell 2016;30:595-609.

42. Oral EA, Reilly SM, Gomez AV, Meral R, Butz L, Ajluni N, Chenevert TL, et al. Inhibition of IKKvarepsilon and TBK1 Improves Glucose Control in a Subset of Patients with Type 2 Diabetes. Cell Metab 2017;26:157-170 e157.

Figure Legends

Fig. 1. Saturated fatty acid (SFA)-induced lipotoxicity provokes p62/SQSTM1 phosphorylation in insoluble inclusion bodies. HepG2 cells were treated with BSA (Con), palmitic acid (PA, 500 μM), thapsigargin (Tg, 1μM), bafilomycin A1 (Baf, 100 nM) or PA + verapamil (0.1, 1, or 10 μM) for 9 h and subjected to the following analyses. (A,B) Cells were subjected to immunostaining (A) and immunoblotting (B). Arrows indicate band shifts of p62. (C) PA-untreated (Con) and -treated cell lysates were subjected to immunoprecipitation (IP) using anti-p62 antibody or control IgG. IP complex and whole cell lysates were analyzed by immunoblotting. Background non-specific and IgG chain bands were identified from p62 and ubiquitin blots, respectively, and used as loading controls. Arrows indicate positions of shifted (black) and unshifted (grey) p62 bands. (D) Cells were subjected to serial protein extraction (solubility fractionation) with indicated concentration of Triton X-100 (TX100) or sodium dodecyl sulfate (SDS) and analyzed by immunoblotting with indicated antibodies (left panel) and quantified (right panels). (E,F) Cells were subjected to immunostaining with indicated antibodies (upper panels) and analyzed by line-scan evaluation of each signal across protein inclusions (lower panels). DNA was stained with DAPI (blue). Boxed areas in fluorescence images are magnified in right-most panels. Scale bars, 5 μm. Quantification data are shown as mean ± s.e.m. ***$P < 0.001$ (Student's *t*-test). Arrowheads indicate the exact or nearest position of the protein molecular weight markers (kD).

Fig. 2. SFA induces TBK1 activation and aggregation with phosphorylated p62. HepG2 cells were treated with BSA (Con), palmitic acid (PA, 500 μM), thapsigargin (Tg, 1μM),

bafilomycin A1 (Baf, 100 nM), tunicamycin (Tm, 5 μg/ml), verapamil (Ver, 50 μM), nicardipine (Nic, 100 μM), stearic acid (SA, 500 μM), oleic acid (OA, 500 μM), and/or docosahexaenoic acid (DHA, 500 μM) for 9 h, followed by immunoblotting (A-D), immunoblot quantification (C,D; lower panels) and immunostaining (E,F). Immunostained images of PA-treated cells (upper panels) were analyzed by line-scan evaluation of each signal across protein inclusions (lower panels). Scale bars, 5 μm. Quantification data are shown as mean ± s.e.m. $^{**}P < 0.01$ (Student's *t*-test). Arrowheads indicate the exact or nearest position of the protein molecular weight markers (kD).

Fig. 3. TBK1 mediates SFA-induced p62 phosphorylation and aggregation into ubiquitinated protein inclusions. (A,B) HepG2 cells were treated with BSA (Con), PA (500 μM), BSA + BX795 (20 μM), PA + BX795, BSA + Amlexanox (Amx, 100 μM), or PA + Amx for 9 h. (A) The cells were lysed, fractionated into 1% Triton X-100-soluble and insoluble fractions, and then subjected to the immunoblotting (left panels) and immunoblot quantification (right panels). (B) Cells with indicated treatments were subjected to immunostaining (upper panel). Boxed areas in fluorescence images are magnified in rightmost panels. Amount of aggregated proteins was quantified (lower panel). Scale bars, 5 μm. (C) HepG2 cells were transduced with shRNA lentiviruses targeting luciferase (sh-Con) or TBK1 (sh-TBK1 #1 and #2) and incubated for 48 h. Then the cells were treated with BSA or PA (500 μM) for 9 h, followed by subcellular fractionation, immunoblotting (upper panel) and immunoblot quantification (lower panels). TBK1 was analyzed from soluble fractions while p62, ubiquitin and β-actin were analyzed from insoluble fractions. All data are shown as mean ± s.e.m. $^{**}P < 0.01$, $^{***}P$

< 0.001 (Student's *t*-test). Arrowheads indicate the exact or nearest position of the protein molecular weight markers (kD).

Fig. 4. The cGAS-STING axis mediates SFA-induced activation of TBK1. At 48 hr after infection with shRNA lentiviruses for luciferase (sh-Con), STING (sh-STING) or cGAS (sh-cGAS#1 and #2), HepG2 cells were treated with BSA (Con) or PA (500 μM) for 9 hr. Then the cells were subjected to immunostaining (A,C), subcellular fractionation and immunoblotting (B,D; left panels) and immunoblot quantification (B,D; right panels). Boxed areas in fluorescence images are magnified in rightmost panels. Immunostained images of PA-treated control cells (A, upper panel) were analyzed by line-scan evaluation of each signal across protein inclusions (A, lower panel). Scale bars, 5 μm. Quantification data are shown as mean ± s.e.m. *$P < 0.05$, **$P < 0.01$ (Student's *t*-test). Arrowheads indicate the exact or nearest position of the protein molecular weight markers (kD).

Fig. 5. Inhibition of TBK1 suppresses p62 phosphorylation and accumulation in livers of obese mice. (A,B) Four-month-old C57BL/6 male mice kept on HFD for 2 months were subjected to daily administration of phosphate-buffered saline (Con, n = 7) or BX795 (25 mg/kg body weight, i.p.; n = 6) for 10 days. LFD-kept mice (n = 5) of the same age were used as a negative control. (C,D) Five-month-old littermate-controlled $Tbk1^{F/F}$ (n=16) and *Albumin-Cre*/$Tbk1^{F/F}$ (n=16) male mice of C57BL/6 background, kept on HFD for 3 months, were analyzed. (A,C) Livers were subjected to solubility fractionation. 1% Triton X-100-soluble and -insoluble fractions were analyzed by immunoblotting and immunoblot quantification. (B,D) Liver sections were subjected to p62 immunostaining.

Hematoxylin counterstaining was used to visualize nuclei. Boxed areas in top panels are magnified in bottom panels. Scale bars, 200 μm. All data are shown as mean ± s.e.m. *P < 0.05, **P < 0.01, ***P < 0.001 (Student's t-test). Arrowheads indicate the exact or nearest position of the protein molecular weight markers (kD).

Fig. 6. Inhibition of TBK1 suppresses NASH-associated p62 phosphorylation and protein inclusion without alleviating hepatosteatosis and liver damage. (A-E) Four-month-old C57BL/6 male mice kept on methionine-restricted choline-deficient (CD)-HFD for 2 months were subjected to daily administration of vehicle (Con, 5% Tween-80 and 5% PEG-400; n = 10) or BX795 (25 mg/kg body weight, i.p.; n = 5) for 10 days. LFD-kept mice (n = 5) of the same age were used as a negative control. (A) Livers were subjected to solubility fractionation. 1% Triton X-100-insoluble fractions were analyzed by immunoblotting (left panel) and immunoblot quantification (right panels). (B,D) Liver sections were subjected to p62 and F4/80 immunostaining, hematoxylin and eosin (H&E) staining, Oil Red O (ORO) staining and Terminal deoxynucleotidyl transferase dUTP Nick-End Labeling (TUNEL) staining. Hematoxylin counterstaining was used to visualize nuclei. Scale bars, 200 μm. Boxed areas are magnified in the insets. (C) Serum ALT levels were quantified. (E) Relative F4/80 expression was quantified through RT-PCR. All data are shown as mean ± s.e.m. NS, not statistically significant; *P < 0.05, **P < 0.01, ***P < 0.001 (Student's t-test). Arrowheads indicate the exact or nearest position of the protein molecular weight markers (kD).

Fig. 7. Inhibition of TBK1 suppresses liver fibrosis induced by NASH. (A-E) The mice described in Fig. 6 were also analyzed by the following experiments. (A) Liver sections

were subjected to Sirius Red staining and α-smooth muscle actin (α-SMA) immunostaining. Scale bars, 200 μm. Boxed areas are magnified in the bottom panel. (B) Areas positive for Sirius Red (left panel) or α-SMA fluorescence intensity (right panel) were quantified. (C and D) Total liver lysates were analyzed by immunoblotting (C) and immunoblot quantification (D). (E) Relative mRNA expression was quantified through RT-PCR. All data are shown as mean ± s.e.m. $*P < 0.05$, $**P < 0.01$, $***P < 0.001$ (Student's *t*-test). Arrowheads indicate the exact or nearest position of the protein molecular weight markers (kD).

Fig. 8. Inhibition of TBK1 suppresses hepatic oxidative stress during NASH. (A) Fresh frozen liver sections from mice described in Fig. 6 were analyzed by dihydroethidium (DHE) staining, which visualizes reactive oxygen species (ROS). Scale bars, 200 μm. (B) DHE fluorescence intensity was quantified. Data are shown as mean ± s.e.m. $***P < 0.001$ (Student's *t*-test). (C) During infection, TBK1-dependent p62 phosphorylation induces aggregation of ubiquitinated microorganisms, making them better substrates for autophagy, which leads to quicker microorganism elimination. (D) During obesity and NAFLD, lipotoxic activation of TBK1 signaling provokes the formation of p62-ubiquitin aggregates. Due to autophagy defects, hepatocytes cannot efficiently eliminate these aggregates, leading to the formation of large protein inclusions during NASH. These protein inclusions can provoke sublethal ROS accumulation, which can culminate in the development of fibrosis during NASH. In addition, lipotoxicity may also increase TBK1 signaling in non-hepatocytes, such as hepatic stellate cells and immune cells, which may

contribute to the fibrotic pathologies. Question marks denote the mechanistic connections that still need to be established by future investigations.

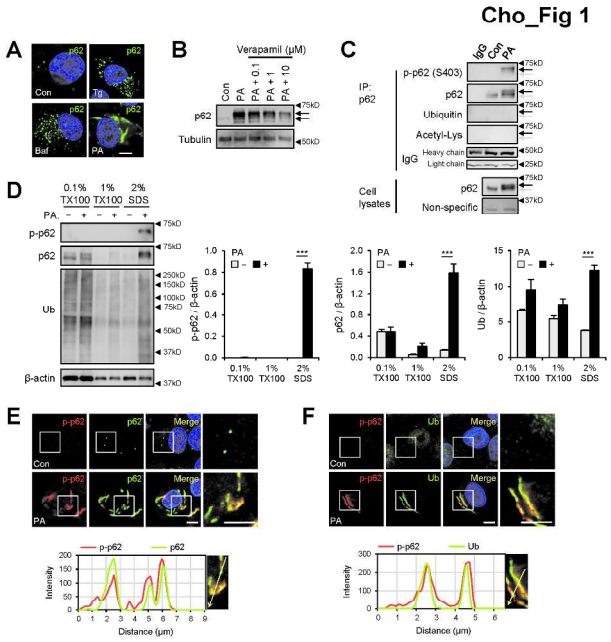

279x215mm (300 x 300 DPI)

Cho_Fig 2

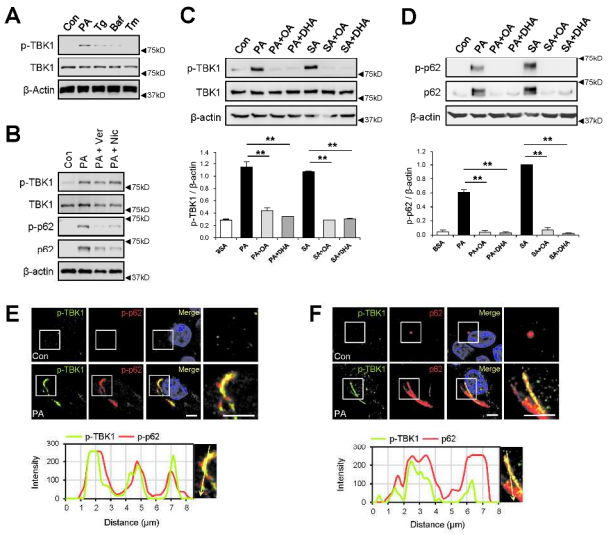

279x215mm (300 x 300 DPI)

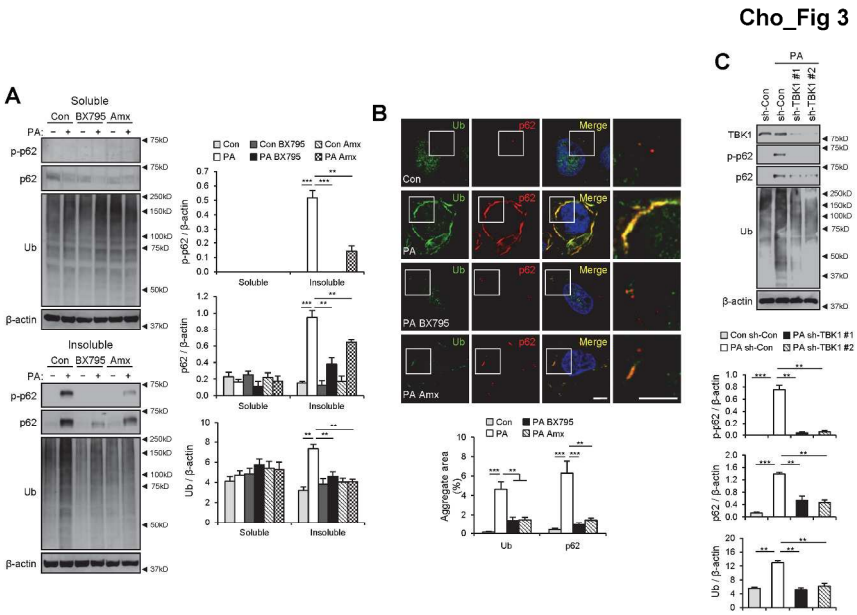

279x215mm (300 x 300 DPI)

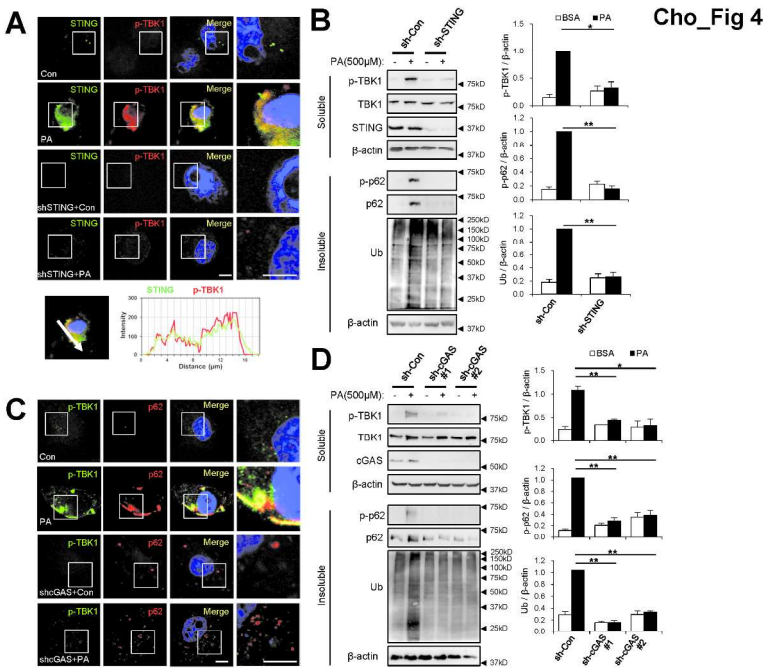

279x215mm (300 x 300 DPI)

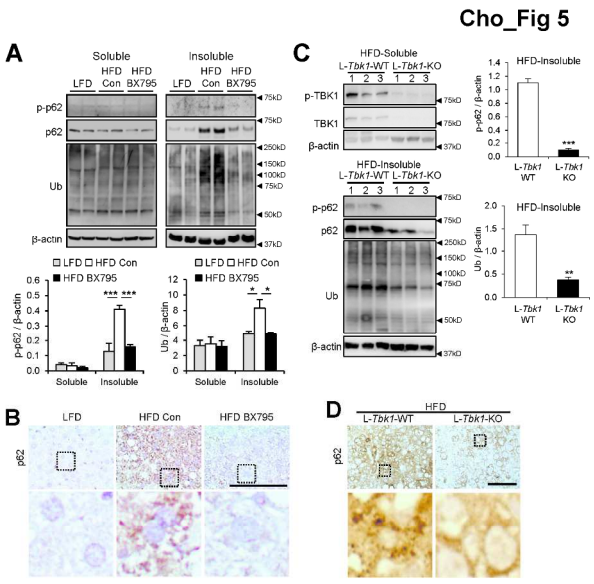

279x215mm (300 x 300 DPI)

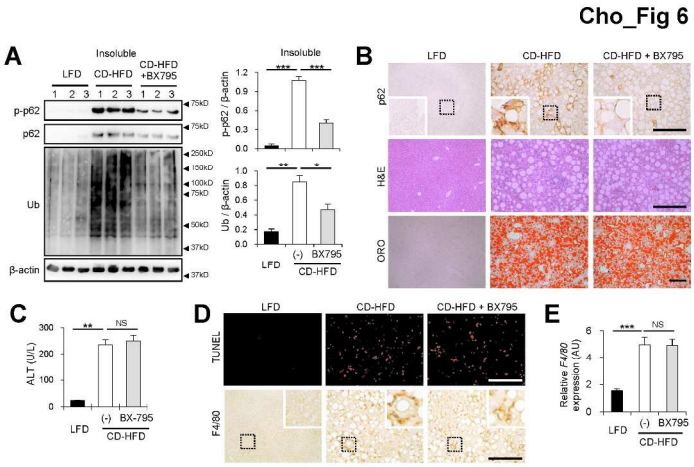

279x215mm (300 x 300 DPI)

Cho_Fig 7

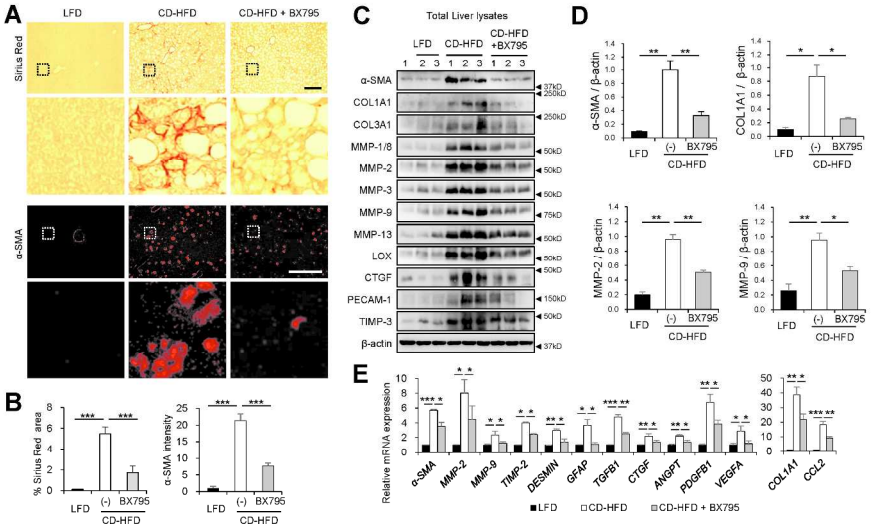

279x215mm (300 x 300 DPI)

Cho_Fig 8

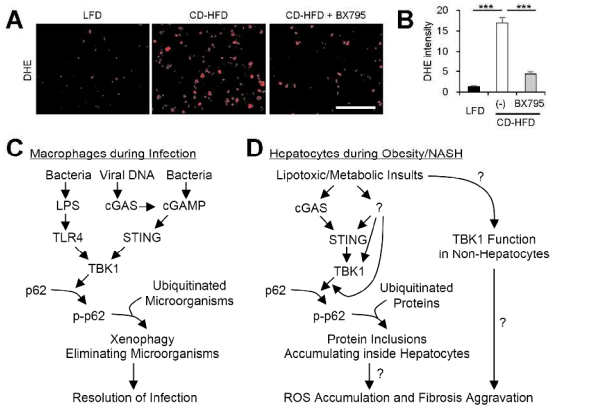

279x215mm (300 x 300 DPI)

Supporting Information

Supporting Materials and Methods

Antibodies and reagents. We obtained ubiquitin (sc-8017), p62/SQSTM1 (sc-28359), LAMP1 (sc-20011), COL1A1 (sc-293182), Pro-COL3A1 (sc-166316), PECAM-1 (sc-376764), MMP-2 (sc-53630), MMP-3 (sc-21732), MMP-9 (sc-393859), MMP-1/8 (sc-137044), LOX (sc-373995), MMP-13 (sc-515284), CTGF (sc-365970), TIMP-3 (sc-373839) and STING (sc-241046) antibodies from Santa Cruz Biotechnology, phospho-Ser403 p62 (MABC186) antibody from Millipore, STING (3337), phospho-Ser172 TBK1 (5483), TBK1 (3013), acetylated lysine (9441), cGAS (15102), LC3 (2775) and p62 (5114) antibodies from Cell Signaling Technology, Actin (JLA20) antibody from Developmental Studies Hybridoma Bank (DSHB), α-smooth muscle actin (ab5694) from Abcam, F4/80 (MF48000) from Invitrogen, Tubulin (T5168) antibody, fatty acid free and low endotoxin bovine serum albumin (BSA), PA, OA, SA, DHA, tunicamycin (Tm), Tg, cGAMP, verapamil and nicardipine from Sigma, BX795 from Selleckchem, amlexanox from Tocris Bioscience, TBBt from Calbiochem, lambda protein phosphatase (λPP) and calf intestine alkaline phosphatase (CIP) from New England Biolabs, and bafilomycin A1 from LC Labs.

Cell culture. HepG2 cells, obtained from ATCC (HB-8065), were cultured in Dulbecco's modified Eagle's medium (DMEM, Invitrogen) containing 10% fetal bovine serum (FBS, Sigma), 50 U/ml penicillin and 50 mg/ml streptomycin. All cultures were maintained in a 37°C incubator with 5% CO_2. The cells were authenticated by Short Tandem Repeat (STR) profiling at ATCC, tested negative for mycoplasma infection, and subcultured for

less than 6 months prior to initiation of the described experiments. Primary hepatocytes were isolated and cultured as previously described.[1] To induce lipotoxicity, de-lipidated low-endotoxin BSA was loaded with PA and other fatty acids, as formerly described,[1,2] and applied to cultured cells.

Mice and diets. Mice of C57BL/6 genetic background were used for the study. *Tbk1*$^{F/F}$ mice (L-*Tbk1*-WT), originally generated by the Takeda Pharmaceutical Company, were crossed with *Albumin-Cre* to generate *Albumin-Cre*/*Tbk1*$^{F/F}$ (L-*Tbk1*-KO) mice. These mice are all in C57BL/6 background, and littermates of L-*Tbk1*-WT and L-*Tbk1*-KO mice were used for the experiments. *Sting*-KO and *cGas*-KO mice are also congenic to the C57BL/6 background and were obtained from the Jackson Laboratory. Mice were maintained in filter-topped cages and given free access to autoclaved regular chow/low-fat diet (LFD, Lab Diet 5L0D), high-fat diet (HFD, Bio-Serv S3282 for the BX795 study and Research Diets D12451 for the L-*Tbk1*-KO study), methionine-restricted choline-deficient HFD (CD-HFD; Research Diets A06071302), methionine-supplemented choline-sufficient HFD (CS-HFD; Research Diets A06071306) and water. A06071302 and A06071306 are identical except the supplemented levels of methionine (0.8g in A06071302 and 5.1g in A0607130, in ~750g diet) and choline (0g in A06071302 and 2g in A0607130, in ~750g diet). In HFD, 45% (D12451) or 60% (S3282, A06071302 and A06071302) of calories come from fat, mostly in the form of lard. In LFD, only 13% (5L0D) of calories come from fat. For diet modulations, 2-month-old male mice raised on LFD were switched to HFD, CD-HFD or CS-HFD diets or kept on LFD for control. Mice were kept on the corresponding diets for two to four additional months. After the diet

modulations, the resulting 4- to 6-month-old mice were analyzed for experiments. When indicated, BX795 (25 mg/kg body weight) was administrated once daily to mice through intraperitoneal (i.p.) injection for the last 10 days before the experiments. Each experiment was done with 5-16 mice per group, and exact animal numbers are indicated in the corresponding figure legends. Exact information regarding mouse age, gender, diet duration, drug dose, route and frequency are also indicated in the corresponding figure legends. All animal studies were ethically approved and overseen by the University Committee on Use and Care of Animals (UCUCA) at the UM.

Lentiviral constructs. The lentiviral plasmids for sh-STING (TRCN0000160895), sh-TBK1 (TRCN0000003182 and TRCN0000003186), sh-cGAS (TRCN0000128706 and TRCN0000148694) and sh-p62 (TRCN0000007234 and TRCN0000007236) were purchased from Open Biosystems. Viruses were generated and amplified in the Vector Core facility at the University of Michigan (UM).

Subcellular Fractionation and Immunoblotting. Cells and tissues were lysed in radioimmunoprecipitation assay (RIPA) buffer or solubility fractionation buffer, and processed as formerly described.[2] In brief, cells and tissues were lysed in a lysis buffer [2] containing 1% Triton X-100. Cell and tissue lysates were centrifuged at 15,000 r.p.m. for 15 min at 4ºC. After centrifugation, pellets were separated from supernatants, resuspended in a lysis buffer containing 2% SDS and boiled in SDS sample buffer (insoluble fraction). Supernatants were also boiled in SDS sample buffer (soluble fraction), and both fractions were analyzed by immunoblotting. For Fig. 1D, cells were initially lysed in a lysis buffer containing 0.1% Triton X-100 so that the lysates were

separated into three fractions. Protein samples were separated by SDS-PAGE, transferred to PVDF membranes and probed with primary antibodies (1:200 for Santa Cruz antibodies, and 1:1,000 for all other antibodies). After incubation with secondary antibodies conjugated with HRP (1:2,000), chemiluminescence was detected using LAS4000 (GE) systems. For the samples analyzed in the same fraction, protein loading amount was normalized to the actin expression level. The degree of phosphorylation-induced gel shift was variable in different gels, and typically more pronounced in gels with extended gel running time. All protein samples were run with the precision plus protein standards (Bio-rad) for molecular weight estimation in the same gel. Exact or nearest positions of protein standards were indicated in all immunoblot images.

Immunocytochemistry. Cells grown on coverslips were fixed with 4% paraformaldehyde and incubated overnight with primary antibodies (1:50 for Santa Cruz antibodies, and 1:400 for all other antibodies). After washing, cells were incubated with Alexa Fluor-conjugated secondary antibodies (Invitrogen, 1:250) for 1.5 hr, counterstained with DAPI (Invitrogen), and analyzed under a laser confocal microscope (Olympus).

Immunoprecipitation. For immunoprecipitation of endogenous p62, cell lysates were prepared in RIPA buffer plus protease inhibitor cocktail (Roche), and incubated overnight at 4°C with anti-p62 antibody (sc-28359) conjugated to a protein G/A bead (Calbiochem). The immunocomplexes were washed three times with the RIPA buffer and then three times with the RIPA buffer plus 0.5 M NaCl, and analyzed through immunoblotting.

Protein identification. Insoluble fraction from PA-treated (9 hr) HepG2 cells was prepared through the method described above. After separation by SDS-PAGE, major protein bands were visualized by Coomassie Blue staining. One of the most prominent bands, appearing around 54kD, was excised from the gel and subjected to the LC-MS/MS analysis at the University of Michigan Proteomics Core facility.

Co-Immunoprecipitation assay. For co-immunoprecipitation between endogenous TBK1 and p62, HepG2 cells were treated with 0.5 mM PA for 3 hr. Then the cells were lysed in 0.3% CHAPS buffer (a lysis buffer[3] containing 0.3% CHAPS) plus protease inhibitor cocktail (Roche), and subjected to immunoprecipitation with control IgG, anti-p62 antibody (sc-28359) or anti-TBK1 antibody (3013, Cell Signaling) conjugated to a protein G/A bead (Calbiochem) overnight at 4°C. The immunocomplexes were washed three times with 0.3% CHAPS buffer and two times with 0.3% CHAPS buffer plus 0.5 M NaCl, and analyzed by immunoblotting.

In vitro kinase assay. Cell lysates were prepared in 0.3% CHAPS buffer plus protease inhibitor cocktail (Roche), and incubated overnight at 4°C with anti-TBK1 antibody (3013, Cell Signaling) conjugated to a protein G/A bead (Calbiochem). After washing three times with 0.3% CHAPS buffer and two times with 0.3% CHAPS buffer plus 0.5 M NaCl, the immunocomplexes were suspended in 50 µl kinase reaction buffer (20 mM Tris-Cl (pH 7.4), 10 mM NaCl, 1 mM DTT, 10 mM $MgCl_2$, and 100 µM ATP) with 1 µg of GST-p62 (BML-UW1035, Enzo Life Sciences) as a substrate and then incubated for 1 hr at 25°C. The reaction was terminated by adding 10 µl 5X SDS sample buffer and incubating the mixture at 95°C for 5 min. The sample was analyzed by immunoblotting.

Quantitative RT-PCR. Total RNA was extracted from tissues or cells using Trizol reagent (Invitrogen), and cDNA was made using MMLV-RT (Invitrogen) and random hexamers (Invitrogen). Quantitative PCR was performed in a Real-Time PCR detection system (Applied Biosystems) with iQ^{TM} SYBR Green Supermix (Bio-rad) and relevant primers. Relative mRNA expression was calculated from the comparative threshold cycle (Ct) values relative to β-Actin. Following primer pairs were used for RT-PCR experiments (5'-3' sequence; F, forward; R, reverse):

α-SMA-F	GTCCCAGACATCAGGGAGTAA
α-SMA-R	TCGGATACTTCAGCGTCAGGA
TGFB1-F	CTCCCGTGGCTTCTAGTGC
TGFB1-R	GCCTTAGTTTGGACAGGATCTG
COL1A1-F	GCTCCTCTTAGGGGCCACT
COL1A1-R	CCACGTCTCACCATTGGGG
GFAP-F	CGGAGACGCATCACCTCTG
GFAP-R	AGGGAGTGGAGGAGTCATTCG
DESMIN-F	GTGGATGCAGCCACTCTAGC
DESMIN-R	TTAGCCGCGATGGTCTCATAC
PDGFB-F	CATCCGCTCCTTTGATGATCTT
PDGFB-R	GTGCTCGGGTCATGTTCAAGT

CTGF-F	GGGCCTCTTCTGCGATTTC
CTGF-R	ATCCAGGCAAGTGCATTGGTA
MMP-2-F	CAAGTTCCCCGGCGATGTC
MMP-2-R	TTCTGGTCAAGGTCACCTGTC
MMP-9-F	CTGGACAGCCAGACACTAAAG
MMP-9-R	CTCGCGGCAAGTCTTCAGAG
TIMP-2-F	TCAGAGCCAAAGCAGTGAGC
TIMP-2-R	GCCGTGTAGATAAACTCGATGTC
CCL2-F	TTAAAAACCTGGATCGGAACCAA
CCL2-R	GCATTAGCTTCAGATTTACGGGT
VEGFA-F	GCACATAGAGAGAATGAGCTTCC
VEGFA-R	CTCCGCTCTGAACAAGGCT
ANGPT1-F	CACATAGGGTGCAGCAACCA
ANGPT1-R	CGTCGTGTTCTGGAAGAATGA
TNF1-F	CCCTCACACTCAGATCATCTTCT
TNF1-R	GCTACGACGTGGGCTACAG
IL10-F	GCTCTTACTGACTGGCATGAG
IL10-R	CGCAGCTCTAGGAGCATGTG

IL6-F	TAGTCCTTCCTACCCCAATTTCC
IL6-R	TTGGTCCTTAGCCACTCCTTC
F4/80-F	CCCCAGTGTCCTTACAGAGTG
F4/80-R	GTGCCCAGAGTGGATGTCT
β-Actin-F	CAAAAGCCACCCCCACTCCTAAGA
β-Actin-R	GCCCTGGCTGCCTCAACACCTC
SRX-F	GCCCAGGGAGGTGACTACTT
SRX-R	GTGGATGCTCCCAGGTACAC
NQO1-F	CGCAGACCTTGTGATATTCCAG
NQO1-R	CGTTTCTTCCATCCTTCCAGG
GSTA1-F	AGCCCAAGCTCCACTACTTCAAT
GSTA1-R	CTTCAAACTCTACTCCAGCTGCAG
SQSTM1-F	ATCGGAGGATCCGAGTGT
SQSTM1-R	TGGCTGTGAGCTGCTCTT
β-Actin (human)-F	CACGAAACTACCTTCAACTCCATC
β-Actin (human)-R	AATGATCTTGATCTTCATTGTGCT

Histology. Liver tissues were fixed in 10% buffered formalin, embedded in paraffin and subjected to immunohistochemical staining, as previously described.[1] In brief, paraffin-embedded liver sections were incubated with primary antibody (Santa Cruz

Biotechnology sc-28359 for p62 staining; 1:100, Invitrogen MF48000 for F4/80; 1:100), followed by incubation with biotin-conjugated secondary antibodies (Vector Lab, BA-9200 for p62; 1:200 or BA-9401 for F4/80; 1:200) and horseradish peroxidase (HRP)-conjugated streptavidin (BD Biosciences, 554066; 1:300). The HRP activity was visualized with diaminobenzidine staining. Haematoxylin counterstaining was applied to visualize nuclei. For α-SMA staining, liver sections were incubated with anti-α-SMA antibody (Abcam ab5694), followed by incubation with Alexa Flour 594-conjugated secondary antibody (Invitrogen). Terminal deoxynucleotidyl transferase dUTP Nick-End Labeling (TUNEL) assay was performed using In Situ Cell Death Detection Kit-TMR-Red (Roche). Dihydroethidium (DHE) staining was performed using freshly frozen liver sections and DHE (Thermo Fisher Scientific, D11347) as formerly described.[4] α-SMA-, TUNEL- and DHE-stained samples were examined under a fluorescence microscope (Meiji). To visualize collagen fibers, liver sections were stained with saturated picric acid containing 0.5% Sirius Red (Sigma). The sections were washed with distilled water, dehydrated, mounted, and examined under a light microscope (Meiji). For Oil Red O staining, OCT-embedded frozen liver sections were allowed to air dry and rinsed with 60% isopropanol, followed by staining with fresh 0.5% Oil Red O solution for 15 min. After staining, the slides were rinsed with 60% isopropanol, washed with distilled water, mounted and analyzed under a light microscope (Meiji).

Serum ALT assay. Serum ALT levels were measured with an ALT (SGPT) activity assay kit (Pointe Scientific, Inc.) according to the manufacturer's instructions.

Supporting Information Figure Legends

Fig. S1. SFA induces p62 phosphorylation and TBK1 activation. (A) KRT8 is one of the major components of palmitic acid (PA)-induced protein inclusion. Insoluble fractions from BSA- and PA-treated HepG2 were analyzed by SDS-PAGE. The band in red box was analyzed by MS/MS and identified as KRT8. (B-F) HepG2 cells (B,D-F) or mouse primary hepatocytes (C) were treated with BSA (Con), PA (500 μM), thapsigargin (Tg, 1μM), bafilomycin A1 (Baf, 100 nM), tunicamycin (Tm, 5 μg/ml) or tetrabromobenzotriazole (TBBt, 50 μM) for 9 h. (B,D,E) Cell lysates were treated with lambda protein phosphatase and calf intestinal phosphatase treatment (λPP+CIP; B) or CIP only (D,E) for 1 hr at 37°C, followed by immunoblotting (B,D) and band quantification (E). Cell lysates were analyzed by immunoblotting (C,F). Quantification data are shown as mean ± s.e.m. $*P < 0.05$, $***P < 0.001$ (Student's t-test). (G-I) HepG2 cells were treated with PA (500 μM) for indicated hours. The cells were then subjected to subcellular fractionation (G,H) or anti-TBK1 immunoprecipitation (IP) (I). Insoluble fraction (G) or indicated fractions (H) were analyzed by immunoblotting. Phosphotransferase activity of immunopurified TBK1 (IP-TBK1) was assayed using recombinant GST-p62 protein and p-p62 antibody (I). (J) PA-treated HepG2 cells (3 hr) were subjected to co-IP assay with normal IgG (-), anti-TBK1 or anti-p62 antibodies. IP complexes were analyzed by immunoblotting. Arrows indicate positions of shifted (black) and unshifted (grey) p62 bands. Arrowheads indicate the exact or nearest position of the protein molecular weight markers (kD).

Fig. S2. STING silencing suppresses SFA-induced protein inclusion formation. At 48 hr after infection with shRNA lentiviruses for luciferase (control) or STING (sh-STING), HepG2 cells were treated with BSA (Con) or PA (500 μM) for 9 hr. Then the cells were subjected to immunostaining. Boxed areas in fluorescence images (A,C) are magnified in rightmost panels. Immunostained images of PA-treated control cells were analyzed by line-scan evaluation of each signal across protein inclusions (B,D). Scale bars, 5 μm.

Fig. S3. cGAS silencing suppresses SFA-induced protein inclusion formation. At 48 hr after infection with shRNA lentiviruses for luciferase (control) or cGAS (sh-cGAS #1), HepG2 cells were treated with BSA (Con) or PA (500 μM) for 9 hr. Then the cells were subjected to immunostaining. Boxed areas in fluorescence images (A,C) are magnified in rightmost panels. Immunostained images of PA-treated control cells were analyzed by line-scan evaluation of each signal across protein inclusions (B,D). Scale bars, 5 μm.

Fig. S4. Extracellular cGAMP treatment activates TBK1 but does not induce p62 phosphorylation. (A,B) HepG2 cells were treated with BSA, PA (500 μM), bafilomycin A1 (Baf, 100 nM) and/or cGAMP (10-20 μM) for 9 h. Then the cells were subjected to subcellular fractionation and immunoblotting. Arrowheads indicate the exact or nearest position of the protein molecular weight markers (kD).

Fig. S5. cGAS-STING pathway mediates lipotoxic activation of TBK1 and subsequent phosphorylation of p62. Primary hepatocytes were isolated and cultured from two-month-old WT, *Sting*$^{-/-}$ and *cGas*$^{-/-}$ mice (n=6, 3 and 3, respectively). The cells were treated with BSA (Con) or PA (500 μM) for 9 hr. Then the cells were subjected to immunostaining

(A,B), subcellular fractionation and immunoblotting (C,D), and immunoblot quantification (E,F). Boxed areas in fluorescence images (A,B) are magnified in rightmost panels. Scale bars, 5 μm (A,B). All data are shown as mean ± s.e.m. $^{**}P < 0.01$, $^{***}P < 0.001$ (Student's *t*-test). Arrowheads indicate the exact or nearest position of the protein molecular weight markers (kD).

Fig. S6. SFA induces expression of Nrf2 target genes through the TBK1 signaling**.** (A-D) At 48 hr after infection with shRNA lentiviruses for indicated genes, HepG2 cells were treated with BSA or PA (500 μM) for 9 hr. Then mRNA expression of indicated genes was examined through quantitative RT-PCR. Quantification data are shown as mean ± s.e.m. $^{***}P < 0.001$ between PA-treated sh-Luc and indicated groups (Student's *t*-test). (E) At 48 hr after infection with shRNA lentiviruses for luciferase (sh-Con) or p62 (sh-p62 #1 and #2), HepG2 cells were treated with BSA or PA (500 μM) for 9 hr. Then the cells were subjected to immunoblotting. Arrowheads indicate the exact or nearest position of the protein molecular weight markers (kD).

Fig. S7. TBK1 inhibitors alleviate SFA-induced autophagic arrest. HepG2 cells were treated with BSA (Con), PA (500 μM), PA + BX795 (20 μM), PA + Amlexanox (Amx, 100 μM) for 9 h. Then the cells were subjected to immunostaining with LC3 (green, an autophagosome marker) and LAMP1 (red a lysosome marker) antibodies (A). DNA was stained with DAPI (blue). Co-localization between LAMP1 and LC3 (B), as well as LC3-covered fluorescent area (C), were quantified. Boxed areas in fluorescence images are magnified in right-most panels (A). Scale bars, 5 μm. Data are shown as mean ± s.e.m. $^{*}P < 0.05$ (Student's t test).

Fig. S8. Effects of TBK1 inhibition on body weight. Mouse cohorts described in Fig. 5 were analyzed for body weight (A,C,D) and food consumption (B). (A,B) During daily administration of PBS and BX795, body weight (A) and daily food consumption (B) of the mice described in Fig. 5A,B were examined. (C,D) Body weights of the mice described in Fig. 5C,D were examined before (C; 2-month-old mice) and after (D; 5-month-old mice) HFD feeding. Data are shown as mean ± s.e.m.

Fig. S9. CD-HFD induces strong p62 phosphorylation and accumulation of ubiquitin-p62 inclusions. (A-D) 2-month-old C57BL/6 male mice kept on LFD were kept on LFD or switched to methionine-restricted choline-deficient diet (CD-HFD) and methionine-supplemented choline-sufficient diet (CS-HFD) for an additional 2 months. The resulting 4-month-old mice were analyzed. (A) Liver sections were subjected to Sirius Red staining, hematoxylin and eosin (H&E) staining, and Oil Red O (ORO) staining. (B) Body weight was monitored throughout the diet modulation. (C) Serum ALT levels were quantified. (D) Livers were subjected to solubility fractionation. 1% Triton X-100-insoluble fractions were analyzed by immunoblotting. (E-G) Mouse cohorts described in Fig. 6-7 were analyzed for body weight (E) throughout the course of experiment. Vehicle and BX795 were only administered in the last 10 days of the experiment. (F) ORO staining area and TUNEL fluorescence intensities were quantified. (G) Relative mRNA expressions were quantified through RT-PCR. All data are shown as mean ± s.e.m. NS, not statistically significant; *$P < 0.05$, **$P < 0.01$, ***$P < 0.001$ (Student's *t*-test). Arrowheads indicate the exact or nearest position of the protein molecular weight markers (kD).

Fig. S10. Involvement of STING in HFD-induced p62 phosphorylation and aggregation. (A-E) Six-month-old WT and *Sting*$^{-/-}$ male mice (n=5) of C57BL/6 background, kept on HFD for 4 months, were analyzed. Livers were subjected to solubility fractionation. 1% Triton X-100-soluble and -insoluble fractions were analyzed by immunoblotting (A) and immunoblot quantification (B,C; mean ± s.e.m.). Body weights of the mice were examined before (D; 2-month-old mice) and after (E; 6-month old mice) HFD feeding. (F-H) Four-month-old WT (n=7) and *Sting*$^{-/-}$ (n=8) male mice of C57BL/6 background, kept on CD-HFD for 2 months, were analyzed. Livers were subjected to solubility fractionation, and 1% Triton X-100-insoluble fractions were analyzed by immunoblotting (F) and immunoblot quantification (G; mean ± s.e.m.). Mouse cohorts were analyzed for body weight (H; mean ± s.e.m.) throughout the course of experiment. **P* < 0.05, ***P* < 0.01 (Student's *t*-test).

Supporting Information References

1. Park HW, Park H, Ro SH, Jang I, Semple IA, Kim DN, Kim M, et al. Hepatoprotective role of Sestrin2 against chronic ER stress. Nat Commun 2014;5:4233.

2. Park HW, Park H, Semple IA, Jang I, Ro SH, Kim M, Cazares VA, et al. Pharmacological correction of obesity-induced autophagy arrest using calcium channel blockers. Nat. Commun. 2014;5:4834.

3. Lee JH, Budanov AV, Park EJ, Birse R, Kim TE, Perkins GA, Ocorr K, et al. Sestrin as a feedback inhibitor of TOR that prevents age-related pathologies. Science 2010;327:1223-1228.

4. Park EJ, Lee JH, Yu GY, He G, Ali SR, Holzer RG, Osterreicher CH, et al. Dietary and genetic obesity promote liver inflammation and tumorigenesis by enhancing IL-6 and TNF expression. Cell 2010;140:197-208.

Cho_Fig S1

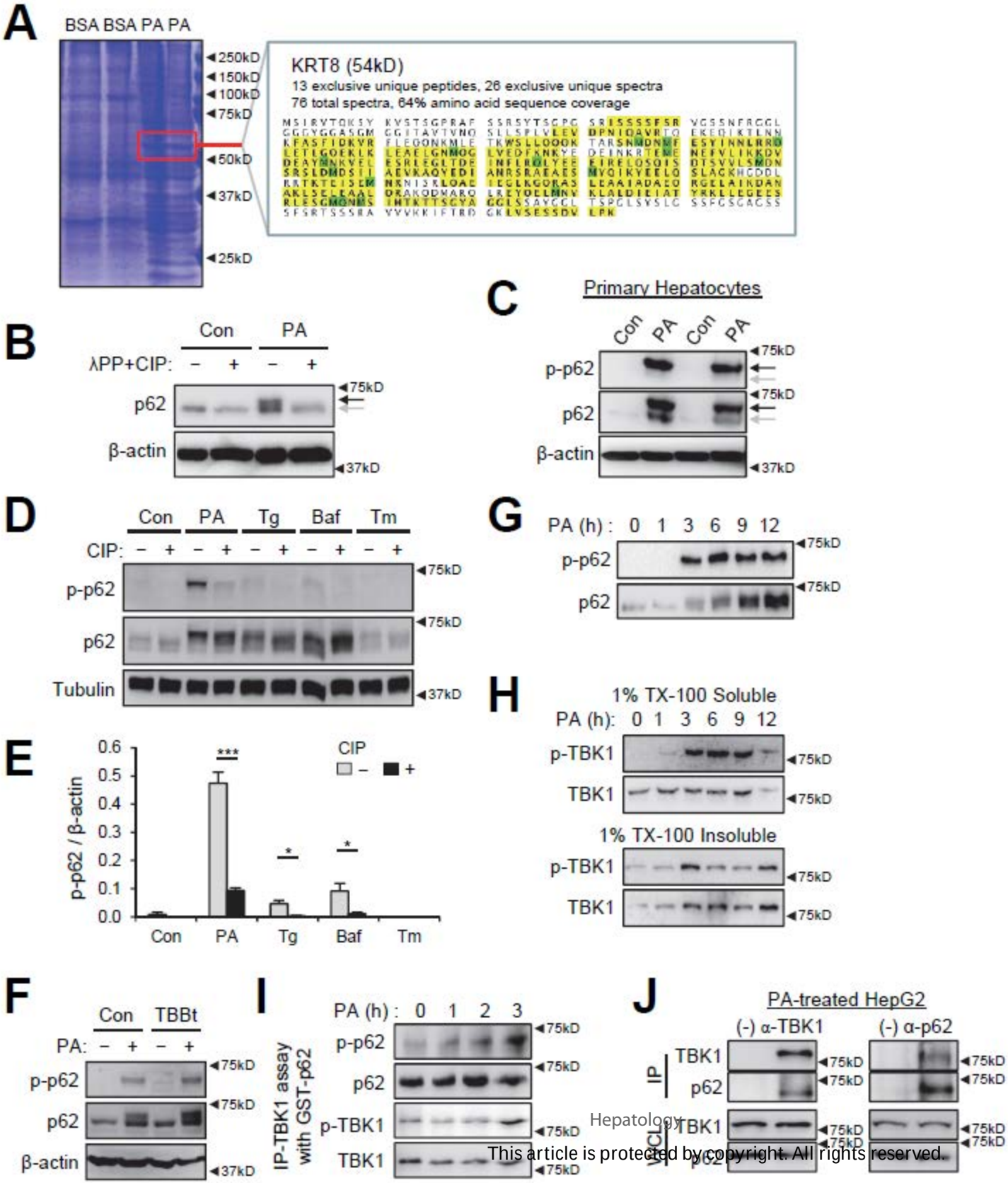

Cho_Fig S2

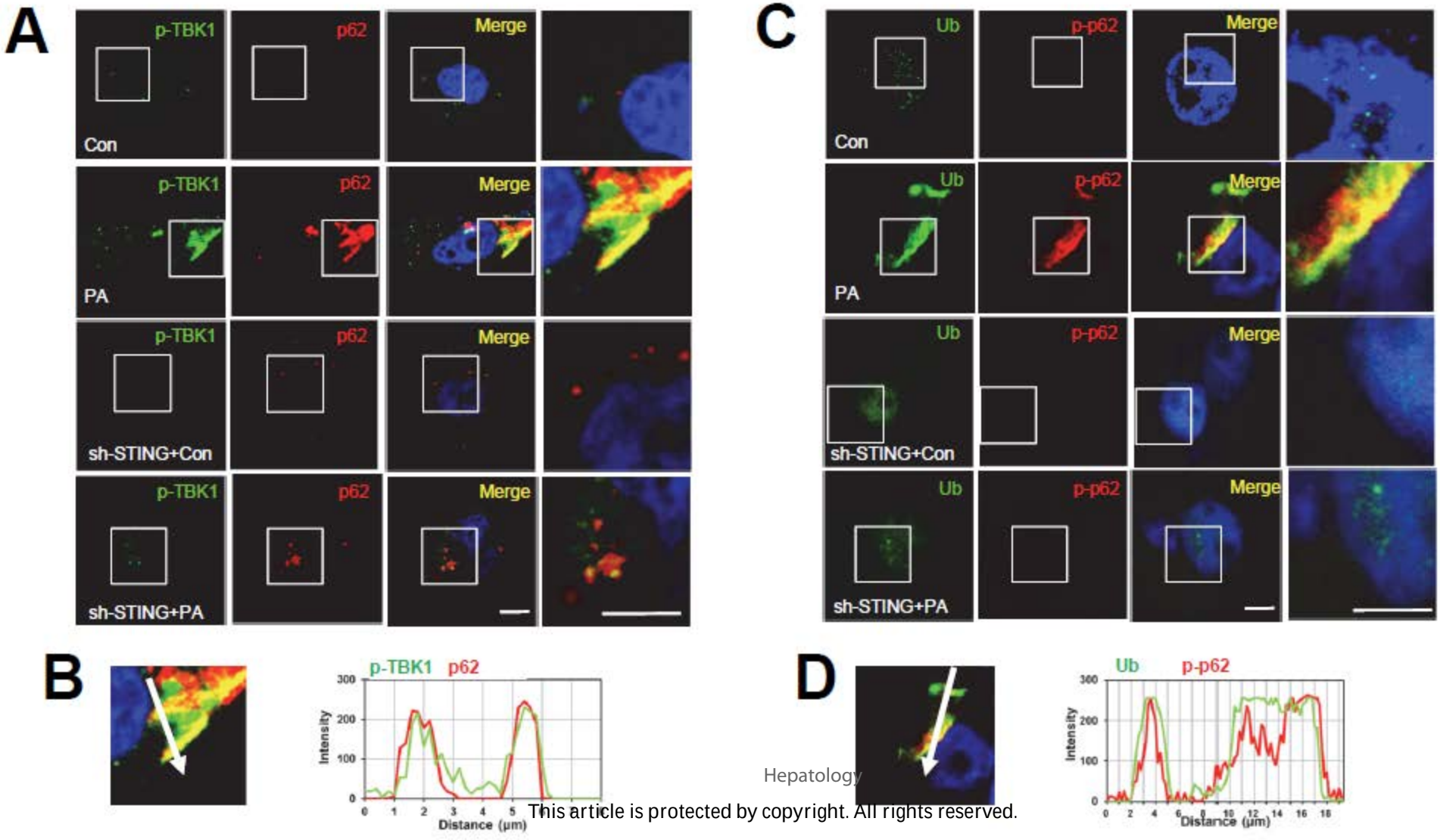

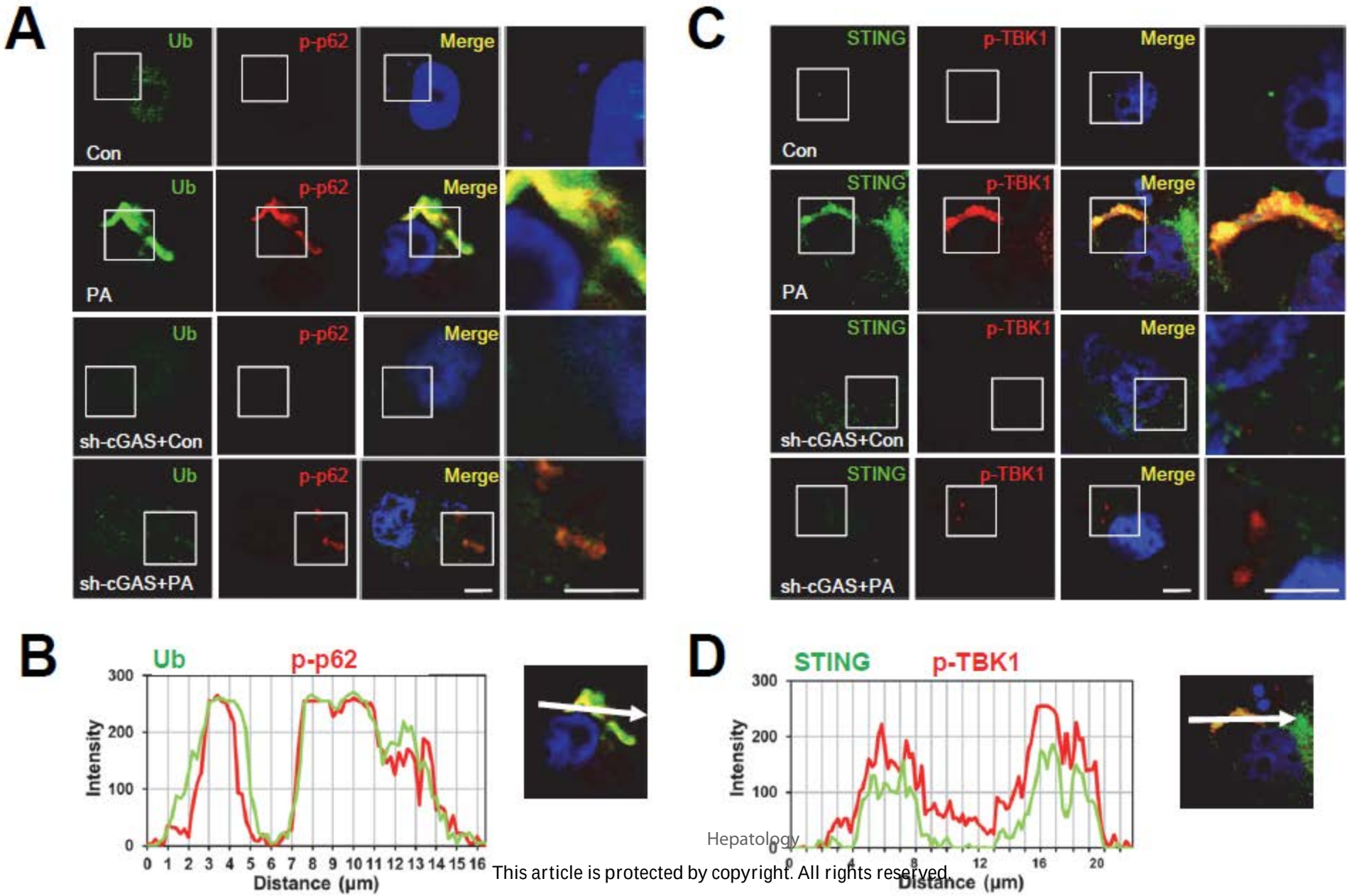

Cho_Fig S4

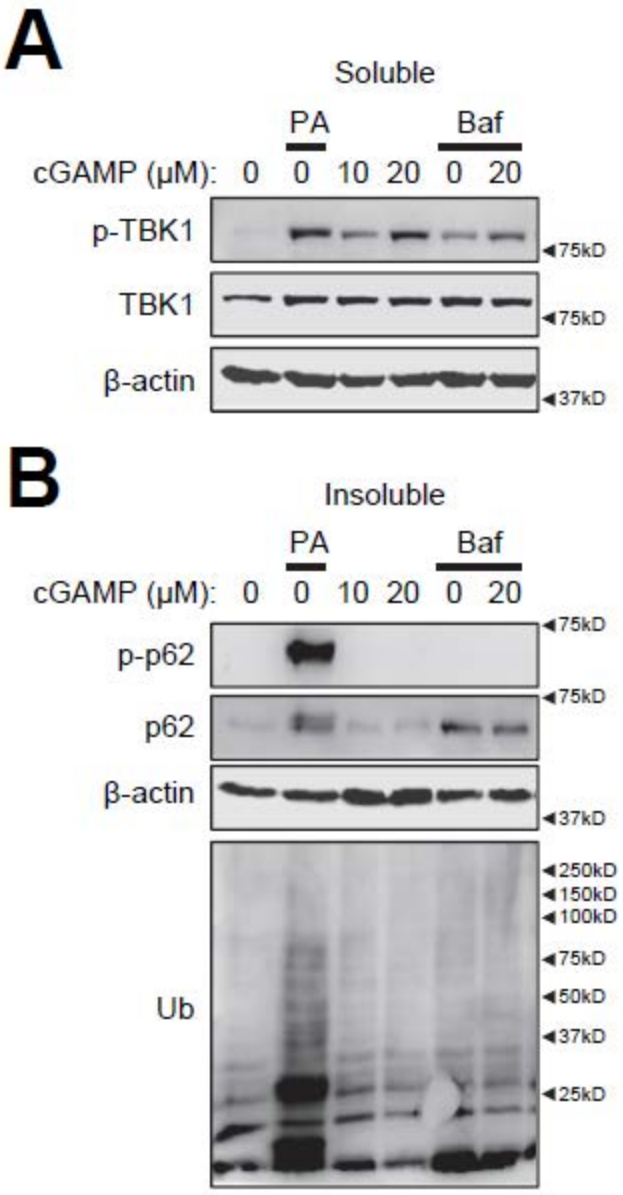

Cho_Fig S5

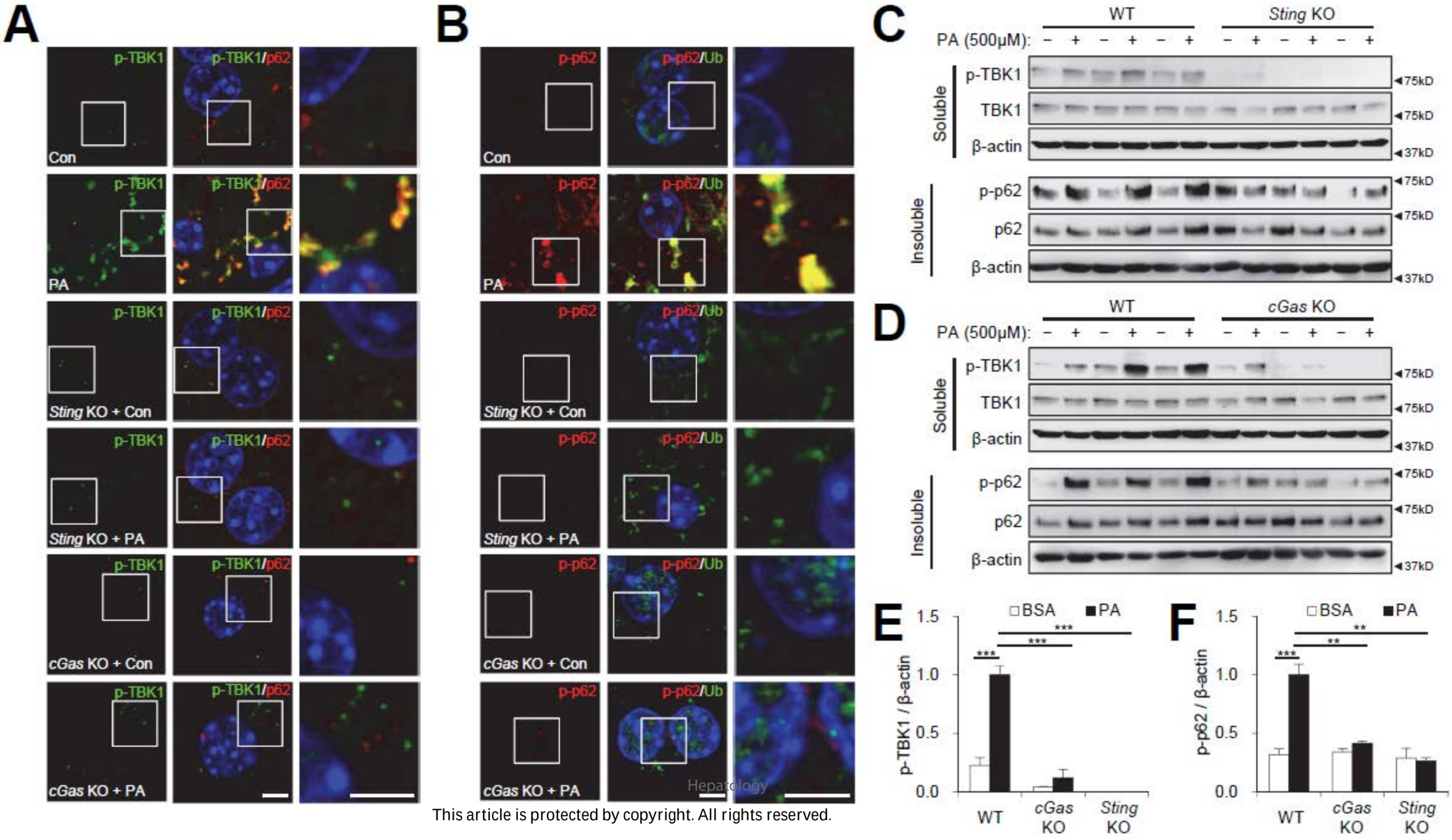

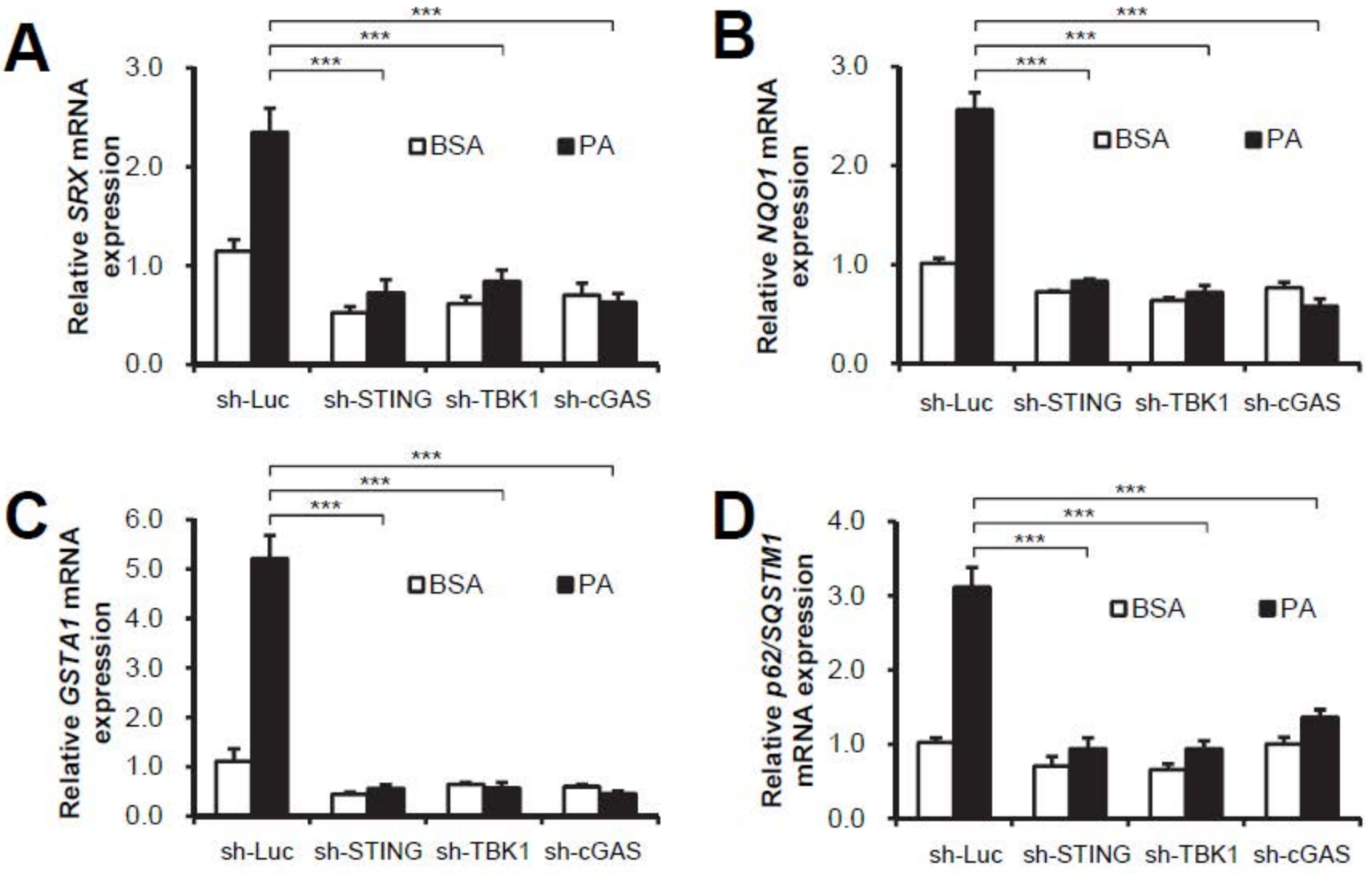

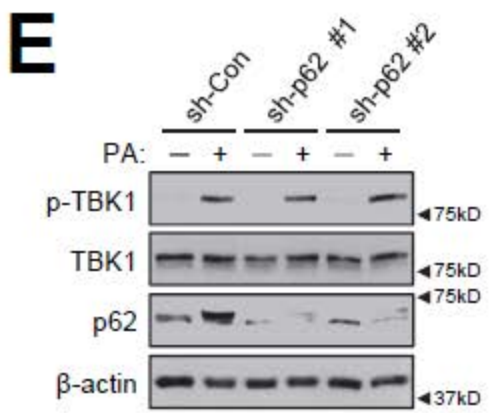

Cho_Fig S7

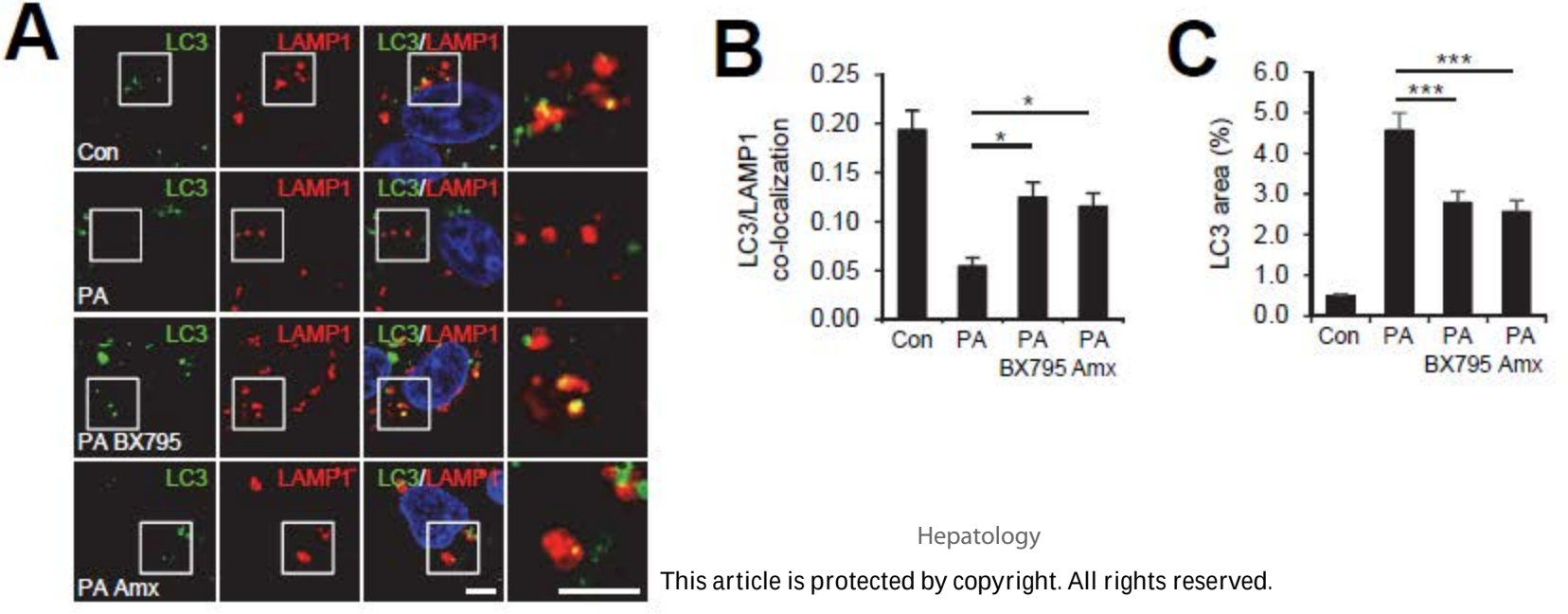

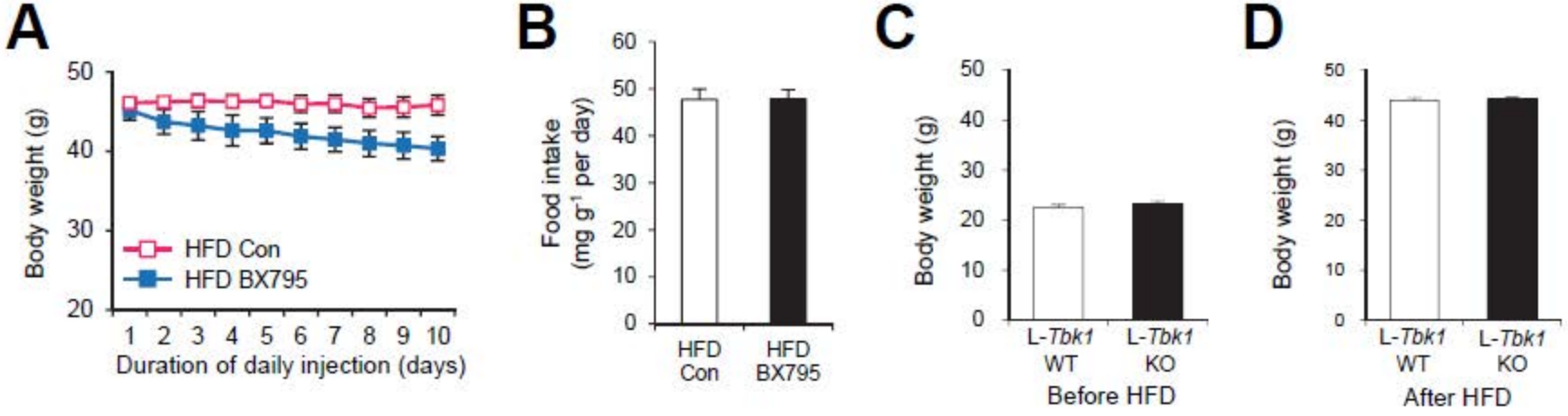

Cho_Fig S9

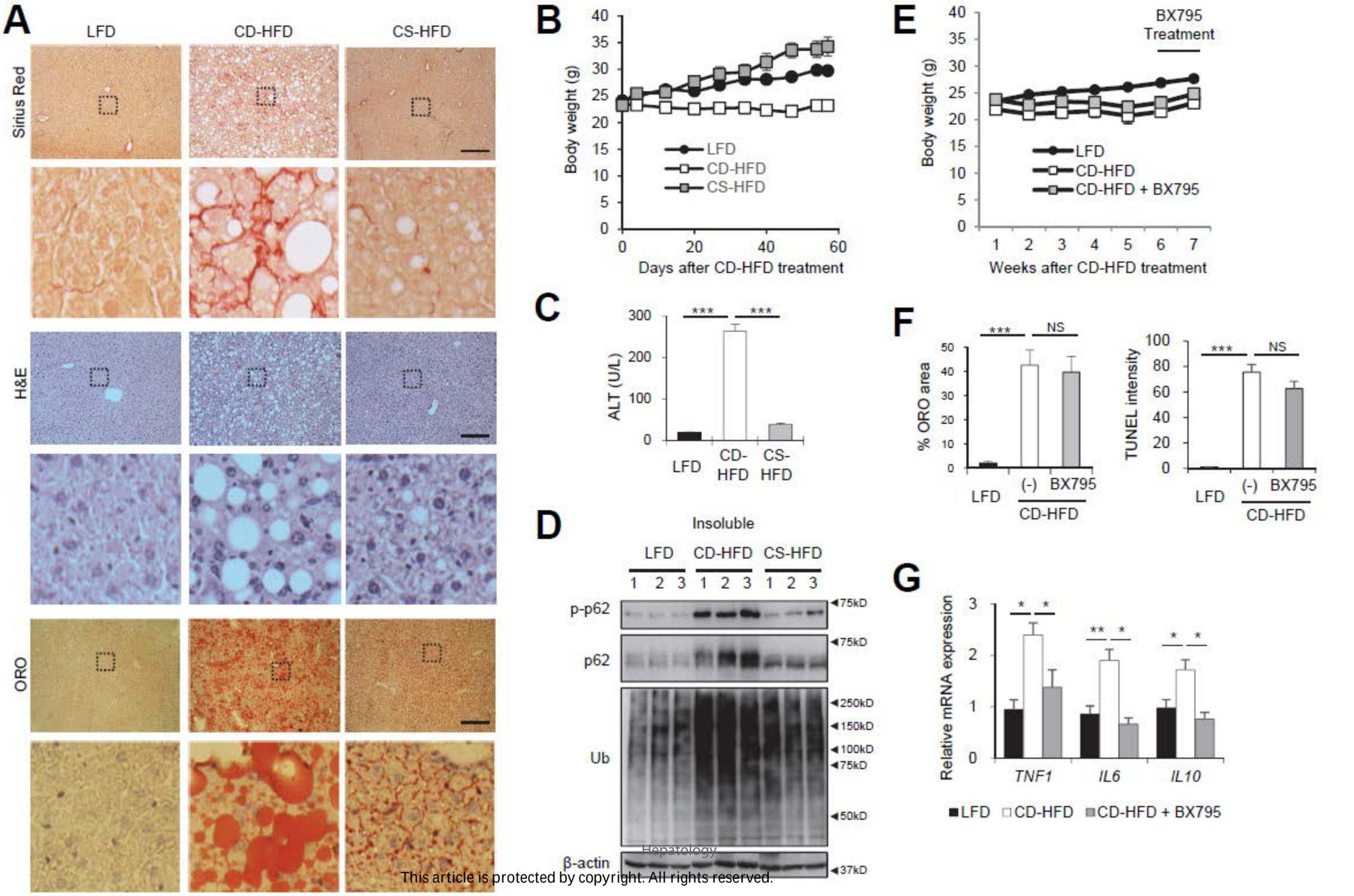

Cho_Fig S10